Endothelial cells elicit a pro-inflammatory response to SARS-CoV-2 without productive viral infection

Running Title: Blood vessels are not infected by SARS-CoV-2.

Lilian Schimmel[1*] Keng Yih Chew[2*] Claudia Stocks[1,3] Teodor Yordanov[1] Patricia Essebier[1] Arutha Kulasinghe[4,5] James Monkman [4,5] Anna Flavia Ribeiro dos Santos Miggiolaro[6] Caroline Cooper[7] Lucia de Noronha[8] Anne K. Lagendijk[1] Kate Schroder[1,3] Larisa I. Labzin[1,3#] Emma J. Gordon[1#] & Kirsty R. Short[2#]

1. Division of Cell and Developmental Biology, Institute for Molecular Bioscience, The University of Queensland, Brisbane, QLD, Australia
2. School of Chemistry and Molecular Biosciences, The University of Queensland, Brisbane, QLD, Australia
3. IMB Centre for Inflammation and Disease Research, Institute for Molecular Bioscience, The University of Queensland, Brisbane, QLD, Australia
4. Queensland University of Technology, School of Biomedical Sciences, Faculty of Health, Brisbane, Queensland, Australia.
5. Translational Research Institute, Brisbane, Queensland, Australia.
6. Postgraduate Program of Health Sciences, School of Medicine, Hospital Marcelino Champagnat - Pontifícia Universidade Católica do Paraná (PUCPR), Brazil
7. Pathology Queensland, Princess Alexandra Hospital, Brisbane, Qld, Australia
8. School of Medicine & Center of Education, Research and Innovation – Hospital Marcelino Champagnat - Pontifícia Universidade Católica do Paraná (PUCPR). Brazil

*/# authors contributed equally

Correspondence:

k.short@uq.edu.au

e.gordon@imb.uq.edu.au

ABSTRACT

Objectives: Thrombotic and microvascular complications are frequently seen in deceased COVID-19 patients. However, whether this is caused by direct viral infection of the endothelium or inflammation-induced endothelial activation remains highly contentious. Methods: Here, we use patient autopsy samples, primary human endothelial cells and an *in vitro* model of the pulmonary epithelial-endothelial cell barrier to show that primary human endothelial cells express very low levels the SARS-CoV-2 receptor ACE2 and the protease TMPRSS2. Results: Accordingly, endothelial cells can only be infected when SARS-CoV-2 is present at very high concentrations. However, this is not a productive infection (i.e. no infectious virus is produced) and viral entry induces an inflammatory response. We also show that SARS-CoV-2 does not infect endothelial cells in 3D vessels under flow conditions. We further demonstrate that in a co-culture model endothelial cells are not infected with SARS-CoV-2. They do however sense and respond to infection in the adjacent epithelial cells, increasing ICAM-1 expression and releasing pro-inflammatory cytokines. Conclusions: Taken together, these data suggest that *in vivo,* endothelial cells are unlikely to be infected with SARS-CoV-2 and that infection is only likely to occur if the adjacent pulmonary epithelium is denuded (basolateral infection) or a high viral load is present in the blood (apical infection). In such a scenario, whilst SARS-CoV-2 infection of the endothelium can occur, it does not contribute to viral amplification. However, endothelial cells are still likely to play a key role in SARS-CoV-2 pathogenesis by sensing adjacent infection and mounting a pro-inflammatory response to SARS-CoV-2.

Keywords: SARS-CoV-2, endothelial cells, COVID-19, inflammation, blood vessels.

52 **INTRODUCTION**

53 SARS-CoV-2 causes diverse clinical syndromes, ranging from asymptomatic infection to fatal disease.
54 Of patients hospitalised with COVID-19 (the clinical manifestation of SARS-CoV-2 infection),
55 approximately 30% of individuals go on to develop severe disease associated with progressive lung
56 damage [1]. This is associated with a breakdown of the vascular barrier, oedema, endotheliitis,
57 thrombosis and inflammatory cell infiltration [1, 2]. Many studies have identified thrombotic and
58 microvascular complications in deceased patients, suggesting that vascular pathology is a major driver
59 of severe disease [3, 4]. Other major pathological events include arterial and
60 venous thromboembolism, kidney disease and neurological disorders [5, 6], suggesting that SARS-CoV-2
61 activates the vasculature throughout the body, potentially resulting in multi-organ failure. However,
62 whether this is caused by direct viral infection of the endothelium or inflammation-induced endothelial
63 activation remains highly contentious.

64

65 SARS-CoV-2 cellular uptake is mediated by binding of the spike glycoprotein to ACE2 (angiotensin-
66 converting enzyme 2) and NRP1 (Neuropilin-1) at the cell surface [7-10]. Host surface proteases such
67 as TMPRSS2 cleave full-length spike protein (S0) at its S2' site. Cleavage at the S2' site can facilitate
68 the fusion of viral and cellular membranes to deliver the viral RNA into the cytosol [1, 11]. Alternative
69 routes of virus uptake have also been reported in cells with low expression of TMPRSS2: this involves
70 endo-lysosomal pathway and cathepsins [12]. Numerous studies suggest that endothelial cells express
71 ACE2 [3, 13-17], Neuropilin receptors [18-22] and TMPRSS2 [23], suggesting that viral infection of endothelial
72 cells is theoretically possible. However, others have suggested that ACE2 is highly expressed in
73 microvascular pericytes [14, 24, 25] and that pericyte injury in response to viral infection may lead to
74 endothelial dysfunction.

75

76 Evidence regarding direct infection of the endothelium with SARS-CoV-2 remains equivocal [26, 27].
77 Autopsy studies on COVID-19 patients have suggested the presence of viral particles in the vascular
78 beds of different organs [3, 28, 29] and others have shown SARS-CoV-2 infection of cultured endothelial
79 cells [30, 31] and human blood vessel organoids [32]. Autopsy studies of deceased COVID-19 patients have

also shown SARS-CoV-2 RNA to be enriched in pulmonary endothelial cells [33]. In contrast, several studies have failed to find evidence of endothelial infection in deceased COVID-19 patients [27] and called into question the validity of identifying virally-infected cells based on the presence of the SARS-CoV-2 spike protein [25, 34, 35]. Animal models of SARS-CoV-2 infection have also failed to identify any obvious signs of endothelial infection [36, 37], despite clear endothelial dysfunction and thrombosis [38].

When and how endothelial cells may be exposed to SARS-CoV-2 *in vivo* also remains unclear. As a respiratory virus, SARS-CoV-2 encounters pulmonary epithelial cells prior to any interaction with the endothelium. SARS-CoV-2 infects pulmonary epithelial cells apically and new viral particles are also released apically into the lumen of the lung [39]. It is possible that the infected epithelial layer loses barrier function, allowing endothelial infection from the basolateral side of epithelia that is adjacent to alveolar endothelium. Alternatively, SARS-CoV-2 may infect endothelial cells apically via the blood, although viremia appears to be rare in COVID-19 patients [40]. The question therefore remains whether endothelial dysfunction in COVID-19 is the result of direct viral infection of the endothelium.

Here, using patient autopsy samples and *in vitro* models, we show that whilst SARS-CoV-2 can enter endothelial cells if high viral titres are present, this infection is not productive. Rather, in response to direct or indirect viral exposure, endothelial cells mount a pro-inflammatory response characterised by increased expression of ICAM-1 and secretion of CXCL-10 and IL-6. Taken together, our results provide clarification on the intensely debated topic of endothelial infection by SARS-CoV-2, to reveal that the endotheliopathy and thrombocytopathy in patients with severe COVID-19 is likely to be due to the inflammatory response, rather than direct viral infection.

108 **MATERIALS AND METHODS**

109 *In vivo samples:* Lung tissue from 10 SARS-CoV-2 infected patients was sectioned and Hematoxylin
110 and Eosin (H&E) staining performed. RNAscope probes (ACDbio, US) targeting SARS-CoV-2 spike
111 mRNA (#848561-C3), were used as per manufacturer instructions for automation on Leica Bond RX.
112 DNA was visualised with Syto13, and SARS-CoV-2 spike probe with opal 690 (1:1500). Fluorescent
113 images were acquired with Nanostring Mars prototype DSP at 20x. Autopsy and biopsy materials were
114 obtained from the Pontificia Universidade Catolica do Parana PUCPR the National Commission for
115 Research Ethics (CONEP) under ethics approval numbers 2020001792/30188020.7.1001.0020 and
116 2020001934/30822820.8.000.0020. The study was also approved under University of Queensland
117 HREC ratification.

118

119 *Cell culture:* Human umbilical vein endothelial cells (HUVECs), and human microvascular endothelial
120 cells from lungs (HMVEC-L) purchased from Lonza (Cat# CC-2935, and CC-2527 respectively) were
121 cultured until passage 8 in EGM-Plus or EGM-2MV medium, supplemented with singlequots (Lonza
122 Cat# CC-5035, CC-3102). Calu-3 cells purchased from ATCC (Cat# HTB-55) were maintained in
123 MEM (Invitrogen), containing 10% (v/v) heat-inactivated foetal bovine serum (Cytiva), 100 U/ml
124 penicillin and streptomycin (Life Technologies Australia), and grown in EGM-2MV for endothelial co-
125 culture experiments. Baby hamster kidney cells (BHK-21) were a kind gift from Prof. Dr. R.G. Parton.
126 Cell lysates of human nasal epithelial cells (HNEp) were a kind gift from Prof. Peter Sly.

127

128 Monocultures of HUVEC, HMVEC or Calu-3 cells were performed on 24 well cell culture inserts
129 (Corning 6.5 mm Transwell, 0.4 µm polycarbonate membrane Cat#3413) coated with 5 µg/ml
130 fibronectin (FN) (Sigma). Approximately 25,000 HUVEC, 25,000 HMVEC and 50,000 Calu-3 cells
131 were seeded per insert on either the apical or basolateral side as indicated and grown in EGM-Plus
132 (Lonza), EGM-2MV (Lonza) or MEM (Invitrogen) respectively. Endothelial cells were treated with
133 100ng/ml TNFα (Life Technologies Australia) or 10ng/ml IFNß (Lonza) for as long as indicated.

134

135 Calu-3 and HMVEC were co-cultured on 24 well cell culture inserts (Corning 6.5 mm Transwell, 0.4
136 µm polycarbonate membrane Cat#3413) coated with 5 µg/ml FN (Sigma) in EGM-2MV (Lonza).
137 Approximately 25,000 HMVECs were seeded on an inverted transwell membrane for 1 hr to attach.
138 Transwell membranes were turned over to normal position and approximately 50,000 Calu-3 cells were
139 seeded in the top compartment of the membrane. Cells were grown for 48 hr prior to infections.
140
141 *Viral infection:* SARS-CoV-2 isolate hCoV-19/Australia/QLD02/2020 was provided by Queensland
142 Health Forensic & Scientific Services, Queensland Department of Health. Virus was grown on Vero
143 cells and titred [41]. Sanger sequencing was used to confirm that no mutations occurred in the spike gene
144 relative to the original clinical isolate. Cells were infected with 6 x 10^4 plaque forming units (PFU) for
145 1 hour at 37 degrees 5% Co2. The viral inoculum was then removed, and the medium was replaced with
146 DMEM (Invitrogen) or MEM (Invitrogen) containing 2% FBS. Alternatively, 2 x 10^6 PFUs were added
147 to the cell culture and cells were incubated at 37 degrees 5% CO_2. All studies with SARS-CoV-2 were
148 performed under physical containment 3 (PC3) conditions and were approved by the University of
149 Queensland Biosafety Committee (IBC/374B/SCMB/2020).
150
151 *Antibodies:* The following antibodies were used: mouse anti-ACE2 (Santa Cruz, sc-390851, IF1:200)
152 goat anti-ACE2 (R&D systems, AF933, WB 1:1000), mouse anti-dsRNA (Millipore, MABE1134,
153 IF1:100), rabbit anti-SARS-CoV nucleocapsid protein/NP (Sino Biological, 40143-R040, WB1:1000
154 IF1:200), rabbit anti-TMPRSS2 (Abcam, ab92323, WB1:1000), rabbit anti-cleaved caspase 3 (Cell
155 Signaling, 9661 IF1:30 after pre-labeling), rabbit anti-GAPDH (Cell Signaling, 2118, WB1:2000),
156 mouse anti-ICAM-1 (R&D systems, BBA3, IF1:200), mouse anti-ICAM-1 (Santa Cruz Biotechnology,
157 sc-8439, WB1:1000), Phalloidin-Alexa555 (Cytoskeleton, PHDH1-A, IF1:500), Phalloidin-Alexa670
158 (Cytoskeleton, PHDN1-A, IF1:200). Pre-labeling of rabbit anti-cleaved caspase 3 with Alexa Fluor 555
159 was performed using Zenon Rabbit IgG labelling kit (Z-25305) according to manufacturer protocol.
160
161 *Immunofluorescence Staining:* Immunofluorescence staining was in general performed on cells
162 cultured on 12 mm glass coverslips or on 24 well cell culture inserts (Corning 6.5 mm Transwell, 0.4

163 µm polycarbonate membrane Cat#3413) coated with 5 µg/ml FN (Sigma), washed with $PBS^{+/+}$(PBS
164 supplemented with 1 mM $CaCl_2$ and 0.5 mM $MgCl_2$), fixed for 10 min in 4% PFA (Sigma), blocked
165 and permeabilized for 30 min with 3% BSA, 0.3% Triton X-100 (Sigma). Primary antibodies were
166 incubated in 1.5% BSA for 1 hr at RT, secondary antibodies linked to Alexa fluorophores (all
167 Invitrogen) were incubated in 1.5% BSA for 1 hr at RT and incubated with 4% PFA (Sigma) for another
168 24 hr in case of SARS-CoV-2 infected cells, after each step samples were washed 3x with $PBS^{+/+}$ and
169 mounted in ProlongGold + DAPI solution (Cell Signaling Technologies, CST 8961S). Z-stack image
170 acquisition was performed on a confocal laser scanning microscope (Zeiss LSM880) using a 40x NA
171 1.3 or 63x NA 1.4 oil immersion objective.
172
173 *3D Microfluidic cell culture:* Microfluidic devices were generated as previously described [42] using
174 2.5mg/ml Collagen (R&D Systems) for the ECM. Cells were seeded 48 hr prior to virus infection and
175 were kept on a rocker at 37C° and 5%CO_2. The tubes were fixed sequentially in 1% formaldehyde,
176 containing 0.05% Triton for 90 sec, followed by 4% formaldehyde for 15 min at 37C°. Tubes were
177 permeabilised with 0.5% Triton for 10 min at 37C° and blocked for 4 hr in 10% goat serum in PBS at
178 4C° prior to staining. Immunofluorescence staining was performed using NP, dsRNA and Phalloidin-
179 Alexa670 antibodies. Z-stack image acquisition was performed on a confocal laser scanning microscope
180 (Zeiss Axiovert 200 inverted microscope with LSM 710 Meta Confocal Scanner) using 40X NA 1.1
181 water immersion objective.
182
183 *Western blotting:* For total cell lysates, cells were washed once with PBS and lysed with RIPA buffer
184 (50 mM Tris, 150 mM NaCl, 1 mM EDTA, 1% Triton X-100, 0.1% SDS, 1% sodium deoxycholate,
185 protease inhibitor, pH 8.0). Pierce BCA protein assay kit (Thermo Scientific) was used to equalize
186 protein amounts and SDS-sample buffer containing 100 mM DTT (Astral Scientific) was added and
187 samples were boiled at 95°C for 10 minutes to denature proteins. Proteins were separated on 4-15%
188 mini protean TGX precast gels (Biorad) in running buffer (200 mM Glycine, 25 mM Tris, 0.1% SDS
189 (pH8.6)), transferred to nitrocellulose membrane (BioRad Cat#1620112) in blot buffer (48 nM Tris, 39
190 nM Glycine, 0.04% SDS, 20% MeOH) and subsequently blocked with 5% (w/v) BSA in Tris-buffered

191 saline with Tween 20 (TBST) for 30 minutes. The immunoblots were analysed using primary antibodies
192 incubated overnight at 4°C and secondary antibodies linked to horseradish peroxidase (HRP)
193 (Invitrogen), and after each step immunoblots were washed 4x with TBST. HRP signals were visualized
194 by enhanced chemiluminescence (ECL) (BioRad) and imaged with a Chemidoc (BioRad).
195
196 *RNA extraction and cDNA synthesis:* RNA was extracted using the Qiagen RNeasy Minikit (Qiagen)
197 or NucleoZOL (BIOKÉ, The Netherlands) according to manufacturer's guidelines. cDNA was
198 synthesized using random hexamers and the high-capacity cDNA reverse transcription kit (Life
199 Technologies) according to the manufacturer's guidelines.
200
201 *Quantitative PCR (qPCR):* qPCR was performed using SYBR Green reagent (Applied Biosystems).
202 All primer sequences are listed in Table 1. qPCR conditions were applied according to the
203 manufacturer's instructions using QuantStudio 6 Flex Real- Time PCR System (ThermoFisher
204 Scientific, Waltham, Massachusetts, MA). HPRT or Glyceraldehyde 3-phosphate dehydrogenase
205 (GAPDH) was used as a housekeeping gene and relative gene expression was determined using the
206 comparative cycle threshold (ΔΔCt) method (Livak, 2001).
207
208 **Table 1: Primers used in the present study**

NAME	SEQUENCE (5'- 3')
SARS-COV2 (MPRO) VIRUS FW	GAGACAGGTGGTTTCTCAATCG
SARS-COV2 (MPRO) VIRUS RV	ACGGCAATTCCAGTTTGAGC
GAPDH FW	CGAGATCCCTCCAAAATCAA
GAPDH RV	TTCACACCCATGACGAACAT
HPRT FW	TCAGGCAGTATAATCCAAAGATGGT
HPRT RV	AGTCTGGCTTATATCCAACACTTCG
ACE2 FW	TCACGATTGTTGGGACTCTGC
ACE2 RV	TCGCTTCATCTCCCACCACT

NEUROPILLIN FW	TGGACCGACCACTCCCAACG
NEUROPILLIN RV	AGAGCCCCAGCCAAATTCACAG
TMPRSS2 FW	GGAAGTTCATGGGCAGCAAG
TMPRSS2 RV	AGGCGAACACACCGATTCTC

Viral titres: Viral titres in cell culture supernatant determined by a plaque assay on Vero cells, according to previously described protocols [41].

Cytokine titres: Cytokine titres in were determined using an Alphalisa kit (Perkin Elmer) according to the manufacturer's instructions. The sum of cytokines detected in the upper and lower compartments of the transwell is shown for each of the monocultured samples, while cytokine levels were kept separated for the upper and lower compartment for the co-cultured samples.

Image analysis: Analysis of immunofluorescent images was performed using ImageJ version 2.0.0-rc-69/1.52n. A mask of the total cell area was created using default intensity threshold on Phalloidin staining. Within the mask, Raw Integrated Density of either ACE2, NP, ICAM-1 was measured, and value was corrected for total mask area resulting in RawIntDen/Area. For dsRNA, MaxEntropy threshold was performed on dsRNA staining to remove background speckles before measuring Raw Integrated Density within the mask. Analysis of Western blot images was performed using Gel Analyzer Tool of ImageJ version 2.0.0-rc-69/1.52n. The background signal was subtracted and values were normalized to corresponding GAPDH loading control. Imaris (Bitplane) version 8 was used to create the XZ projection in Figure 4B''. Extrusion of cells was quantified in Supplemental Figure 1C using orthogonal views in ImageJ version 2.0.0-rc-69/1.52n.

Statistical analysis: All statistical analysis was performed using Graphpad Prism version 9.0. Data are presented as mean±s.e.m. with individual data points indicated and colour coded per independent experimental replicate. Statistical significance was determined using Kruskal Wallis test for multiple

232 comparisons or Mann-Whitney test between mock and SARS-CoV-2 treated conditions. *P<0.05,
233 **P<0.01, ***P<0.001 and ****P<0.0001.
234
235 **RESULTS**
236 **Endothelial cell infection is not readily detected in deceased COVID-19 patients**
237 To determine the prevalence of *in vivo* SARS-CoV-2 endothelial cell infection, autopsy lung sections
238 were obtained from 10 deceased COVID-19 patients and probed for SARS-CoV-2 spike mRNA using
239 RNAscope. Two of the 10 patients were positive for SARS-CoV-2 RNA in the lungs. In these
240 individuals, spike mRNA could not be detected in pulmonary endothelial cells (endothelial cells defined
241 by H & E staining (Figure 1). These data suggest that the endothelium is not generally the primary site
242 of viral replication *in vivo* in COVID-19 patients (patient data available in Supplemental Table 1).
243
244 **Primary endothelial cells express low levels of ACE2 and TMPRSS2**
245 To further investigate the contribution of endothelial cells to the pathogenesis of SARS-CoV-2, we
246 established *in vitro* cultures of primary human umbilical vein endothelial cells (HUVECs) and human
247 microvascular endothelial cells from the lung (HMVEC-L). Multiple studies have reported that
248 endothelial cells across different vascular beds express ACE2 and TMPRSS2, the host cell receptor and
249 protease that are required for efficient cell infection by SARS-CoV-2 [10, 11]. We found that both HUVECs
250 and HMVEC-Ls expressed comparable ACE2 and TMPRSS-2 mRNA to that observed in immortalised
251 epithelial cells known to be susceptible to SARS-CoV-2 infection (Calu-3) (Figure 2A). Neuropilin-1,
252 which enhances viral entry through its interaction with the spike multibasic cleavage site [7, 8], was readily
253 detected in endothelial cells by qPCR (Figure 2A) in line with established data [19]. The expression of
254 ACE2 protein detected by immunofluorescence (Figure 2B) was significantly reduced compared to
255 epithelial cells (Calu-3) (Figure 2C). We also detected ACE2 and TMPRSS2 protein in HUVECs and
256 HMVEC-Ls by western blot (Figure 2D-E). The specificity of our ACE2 antibody was confirmed by
257 western blot of BHK-21 cells (which are known to be negative for ACE2) [43].These data suggest that
258 while vascular endothelial cells can theoretically be infected by SARS-CoV-2, infection is likely to be

259 inefficient compared to epithelial cells, because of weak receptor and protease expression in endothelial
260 cells.
261
262 **Endothelial cells are not productively infected by SARS-CoV-2**
263 SARS-CoV-2 may theoretically enter endothelial cells via the apical surface (should the virus enter the
264 blood stream) or the basolateral surface (should the virus be present at the basolateral surface of the
265 adjacent epithelial cells). We therefore assessed whether endothelial cells were susceptible to SARS-
266 CoV-2 infection when exposed either apically (Supplemental Figure 1A) or basolaterally (Supplemental
267 Figure 1B) to 6 x 10^4 PFUs. Infectious virus was not detected in the supernatant of either HUVECs or
268 HMVEC-Ls at 24, 48 nor 72 hours post-infection (Supplemental Figure 1C). In contrast, Calu-3 cells
269 demonstrated robust viral replication and release (Supplemental Figure 1C). Similarly, no increase in
270 SARS-CoV-2 nucleocapsid protein within infected endothelial cells relative to mock was detected by
271 immunofluorescence (Supplemental Figure 1D-G) or western blot (Supplemental Figure 1H-I), and no
272 detectable alterations in endothelial cell morphology were evident after viral exposure, as assessed by
273 phalloidin immunostaining (Supplemental Figure 1D, F). In contrast, Calu-3 cells displayed a
274 significant increase in nucleocapsid protein expression after viral exposure. Together, these data suggest
275 that endothelial cells *in vitro* are not efficiently infected with SARS-CoV-2.
276
277 We next sought to establish if the low levels of ACE2 and TMPRSS2 on endothelial cells could be
278 overcome by a higher viral titre, to mediate infection. Accordingly, endothelial cells were infected either
279 apically or basolaterally with 2 x 10^6 PFUs of SARS-CoV-2 and viral replication was again assessed
280 over time. Infectious virus did not increase over time in endothelial cells, rather viral titres decreased
281 over time, consistent with a degradation of input virus (Figure 3A). In contrast, productive viral
282 replication was observed in Calu-3 cells over time (Figure 3A, Supplemental Figure 2A), while, as
283 expected, non-susceptible, ACE2-negative BHK-21 cells showed no productive viral replication
284 (Supplemental Figure 2A). To determine if endothelial cells were susceptible to viral entry, if not
285 replication, we assessed viral nucleocapsid protein by immunofluorescence in HMVEC-L (Figure 3B-
286 C) positive control Calu-3 and negative control BHK-21 (Supplemental Figure 2D-E) and western blot

287 (Figure 3E-F, Supplemental Figure 2B-C). Viral nucleocapsid protein expression was significantly
288 increased after both apical and basolateral SARS-CoV-2 infection, revealing that SARS-CoV2 can
289 indeed enter endothelial cells *in vitro*. We observed that the majority of infected, nucleocapsid protein-
290 positive endothelial cells appeared to be extruding from the cell monolayer in an apical manner (Figure
291 3B', 3B'', 3C). These results were not due to dead cells present in the viral inoculum as BHK-21 cells
292 did not show any nucleocapsid-positive extruded cells (Supplemental Figure 2D). Moreover, extruding
293 endothelial cells were positive for cleaved caspase 3, indicating that SARS-CoV-2 entry into endothelial
294 cells induces apoptosis (Figure 3G-H). These results demonstrate that while SARS-CoV-2 can enter
295 endothelial cells this infection is not productive and leads to apoptosis and extrusion of these apoptotic
296 cells from the endothelial monolayer.
297
298 **Endothelial cells are not productively infected by SARS-CoV-2 in 3D vessels**
299 To determine whether endothelial cells can be infected in 3D vessels under flow, we cultured both
300 HMVEC-L and Vero cells in microfabricated tubes [42] and added SARS-CoV2 to the luminal surface
301 (Figure 4A). After 24h, Vero cells were readily infected and viral replication was observed, in contrast
302 to HMVEC-L which shows viral input levels (Figure 4B). In agreement, NP was not detected in
303 HMVEC-L tubes, whereas Vero cells displayed clear NP staining at the luminal surface (Figure 4C-F).
304 This data reveals that fluid flow over endothelial cells does not alter the ability of SARS-CoV-2 to
305 infect cells.
306
307 **Endothelial cells mount a modest immune response to SARS-CoV-2**
308 As severe COVID-19 disease is associated with an elevated cytokine response [44], we sought to assess
309 whether the abortive SARS-CoV-2 infection observed in endothelial cells induces a pro-inflammatory
310 response. We assessed expression of the leukocyte adhesion molecule, ICAM-1, which is well
311 established to be induced under inflammatory conditions in the endothelium [45]. Immunofluorescence
312 showed that HMVEC-L exposed both basally and apically to SARS-CoV-2 significantly increased
313 ICAM-1 expression, except for in nucleocapsid protein-positive HMVEC-L (likely as they are apoptotic
314 and extruded from the monolayer) (Figure 5A-C). The moderate basal ICAM-1 expression observed in

315 mock infected cells is likely due to the fact that the cells are kept for 72h without a media change (as
316 seen in PBS controls (Figure 5B). However, this response was not as robust as when HMVEC-L were
317 exposed to the established inflammatory cytokine TNFα (Figure 5B-C). Western blot analysis
318 confirmed that HMVEC-L exposed to SARS-CoV-2 displayed a trending increase in ICAM-1
319 expression (Figure 5D, E). In addition to upregulating inflammatory adhesion molecules, we analysed
320 whether endothelial cells can be the source of pro-inflammatory cytokines during SARS-CoV-2
321 infection. As IL-6 and CXCL10 are elevated in patients with severe COVID-19 [46], we analysed whether
322 endothelial cells released these pro-inflammatory cytokines when infected either apically or
323 basolaterally with SARS-CoV-2 for 72h. HMVEC-Ls released modest levels of CXCL10 (Figure 5F)
324 and IL-6 (Figure 5G). While these modest levels of cytokine release from endothelial cells upon SARS-
325 CoV-2 infection are lower than CXCL10 or IL-6 induced in response to high concentrations of
326 recombinant TNF or IFNß, (Supplemental Figure 2F-G), this shows that endothelial cells express high
327 basal levels of IL-6 and that both cytokines are increased during infection. Taken together, these results
328 show that endothelial cells do not support a productive SARS-CoV-2 infection but still mount a modest
329 pro-inflammatory response to the virus.
330
331 **Infection of epithelial-endothelial co-cultures elicits an immune response in endothelial cells**
332 To create a more physiologically relevant *in vitro* model of the pulmonary endothelium, we adapted our
333 previously described co-culture model of the lung epithelial-endothelial barrier [47], where epithelial
334 (Calu-3) cells are seeded on top of a transwell membrane while endothelial cells (HMVEC-L) are
335 seeded on the basolateral side (Figure 6C). To mirror a respiratory infection, SARS-CoV-2 was added
336 to the upper compartment and both epithelial and endothelial cells were analysed at 72h post-infection.
337 In contrast to our observations in endothelial cell monocultures, no viral nucleocapsid protein or viral
338 dsRNA was detected in HMVEC-L, whereas SARS-CoV-2 nucleocapsid protein and viral dsRNA
339 (indicating actively replicating virus) was clearly detected in infected Calu-3 cells (Figure 6A,B; 6E,F).
340 These results were confirmed by the presence of higher levels of viral RNA as measured by qPCR in
341 the Calu-3 compared to the HMVEC-L (Fig 6G) and higher titres of infectious virions in the
342 supernatants of the upper (Calu-3) compartment of the transwell (Figure 6H). Despite lack of

343 endothelial infection, we observed that HMVEC-L cells expressed ICAM-1 expression when virus was
344 added to the upper (Calu-3) compartment, suggesting that the HMVEC-L respond to adjacent epithelial
345 infection (Figure 6A, D). These HMVEC-L also responded to the infection in the adjacent Calu-3 cells
346 by increasing CXCL10 secretion (detected in lower compartment of the co-culture) (Figure 6I). Both
347 Calu-3 and HMVEC-L appeared to secrete IL-6 in response to SARS-CoV-2 infection, as IL-6 levels
348 were increased in both compartments (significantly in the upper, trending in the lower) (Figure 6J). In
349 summary, in a co-culture model of the pulmonary epithelium, endothelial cells are not directly infected
350 with the virus, but respond to adjacent epithelial infection by upregulating ICAM-1 expression and
351 releasing pro-inflammatory cytokines. This suggests that endothelial inflammation and dysfunction
352 during *in vivo* SARS-CoV-2 infection is most likely to occur in response to infection of the adjacent
353 epithelial layer.
354
355 **DISCUSSION**
356 SARS-CoV-2 can induce vascular dysfunction and thrombotic events in patients with severe COVID-
357 19. However, the cellular and molecular mechanisms by which SARS-CoV-2 infection triggers such
358 pathologies have so far remained elusive. Here, we have shown that endothelial cells do not support
359 productive replication of SARS-CoV-2, but that they induce pro-inflammatory cytokines and adhesion
360 molecules upon either direct or indirect exposure to SARS-CoV-2 virions. This supports the hypothesis
361 that the endothelial dysfunction observed in COVID-19 patients is likely to be largely mediated by
362 inflammatory signalling pathways.
363
364 As COVID-19 case numbers rose, reports of COVID-19 coagulopathy and vascular dysfunction also
365 began to accumulate. Whether SARS-CoV-2 directly infects the vasculature to drive this vascular
366 pathology has thus remained a topic of intense debate. Multiple studies show viral particles surrounding
367 the vasculature [3, 25, 43], yet it is unclear whether this infection is truly specific to the endothelium or
368 occurs within the perivascular compartment. Our *in vivo* analyses of lung tissue samples from deceased
369 COVID-19 patients indicates the endothelium remains uninfected. Nevertheless, we showed that *in*
370 *vitro,* endothelial cells are theoretically susceptible to SARS-CoV-2 infection, as they express ACE2,

371 TMPRSS2 and NRP1, albeit at significantly lower levels than epithelial cells. This is in line with other
372 studies that showed expression of SARS-CoV-2 receptors by the endothelium in human tissue or in
373 cultured cells [14, 17, 23, 31]. However, we did not detect endothelial cell infection following exposure to 6
374 x 10^4 PFUs of SARS-CoV-2, whereas epithelial cells were readily infected at the same viral dose. These
375 results support those of Wang et al. [31], who showed that epithelial cells are more susceptible to infection
376 than endothelial cells. When exposed to higher viral titres, endothelial cells were positive for viral NP
377 protein, suggesting effective viral entry. However, no infectious virions were detected in the endothelial
378 cell supernatant, indicating that this infection was abortive. It is interesting to speculate as to why
379 SARS-CoV-2 infection is productive in a monoculture of epithelial, but not endothelial cells. This may
380 relate to cell-dependent differences in viral entry. For example, in epithelial cells, there may be
381 sufficient surface TMPRSS2 levels available to cleave the spike protein at the S2' site and mediate
382 viral-host cell membrane fusion. This may in turn allow for efficient release of viral RNA into the
383 cytoplasm and thus viral replication. In contrast, in cells with lower TMPRSS2 expression (such as
384 endothelial cells), SARS-CoV-2 may enter the cell via endocytosis, with S2' cleavage being mediated
385 by endosomal cathepsins [12]. Endosomal entry may not only be inefficient, but it may also activate the
386 cellular anti-viral response and thereby limit productive viral replication [48, 49]. Alternatively, a host of
387 other cellular co-factors expressed preferentially in epithelial cells may support selective SARS-CoV-
388 2 replication, or endothelial-specific restriction factors may limit effective viral replication.
389
390 In contrast to endothelial cells in a monoculture, viral proteins could not be detected in endothelial cells
391 grown in a co-culture with SARS-CoV-2-positive epithelial cells, despite being exposed to the same
392 dose of virus. These data may reflect the fact that SARS-CoV-2 typically infects and buds from
393 epithelial cells in an apical manner, resulting in limited exposure of the endothelium to infectious
394 virions. Extrapolating these data to the *in vivo* situation would suggest that a basolateral (abortive)
395 infection of the endothelium by SARS-CoV-2 is only likely to occur when the epithelial barrier of the
396 lung is severely damaged, exposing the endothelium to incoming virions.
397

398 While endothelial cells (either in a monoculture or in a co-culture) did not produce infectious virions,
399 they did respond to SARS-CoV-2 infection. Analysis of infected endothelial monolayers revealed that
400 cells positive for viral proteins were extruded in an apical fashion, without any apparent disruption to
401 the monolayer, as assessed by phalloidin expression. This is in contrast to work from Buzhdygan and
402 colleagues, who demonstrated that purified SARS-CoV-2 spike protein can induce the breakdown of
403 the vascular barrier in brain microvascular endothelial cells [50]. Discrepancies between these results may
404 be due to different sources of primary endothelial cells (lung versus brain), or the differences in response
405 of the endothelium to a purified viral protein vs infectious virus [1, 3, 24, 29, 51-53]. However, if infected cells
406 are promptly removed from exposed vessels as our data suggests, then this may explain why detection
407 of viral particles in the endothelium of patients has varied between studies [4, 54].
408
409 In the absence of direct endothelial infection, hyperinflammation is likely to contribute to endothelial
410 dysfunction observed in COVID-19 patients. SARS-CoV-2 triggered an upregulation of endothelial
411 ICAM-1 expression when HMVEC-Ls were directly exposed to virus, or co-cultured with infected
412 epithelial cells. ICAM-1 enables immune cells to effectively extravasate into tissues, so its upregulation
413 is in keeping with the observed influx of inflammatory monocytes, neutrophils and other immune cells
414 into the lungs in severe COVID-19 patients [55]. This suggests that locally produced pro-inflammatory
415 cytokines stimulate the endothelium to induce adhesion marker expression. Our previous studies with
416 influenza virus showed that endothelial cells can themselves be a source of these pro-inflammatory
417 cytokines [56], and indeed we also observed SARS-CoV-2-induced release of IL-6 and CXCL10 in co-
418 cultures. Precisely how SARS-CoV-2 is sensed by the endothelium in either the monoculture or co-
419 culture system remains to be determined. Given that SARS-CoV-2 does not replicate in endothelial
420 cells, we speculate that endothelial cells are unlikely to sense this virus through cytosolic RNA receptors
421 such as RIG-I or MDA5, as these immune sensors would detect viral replication intermediates. A more
422 likely scenario is that the endothelial cells respond to danger signals from neighbouring infected
423 epithelial or endothelial cells. These data add to a growing body of literature that indicate that
424 endothelial cell-directed inflammation plays a key role in the pathogenesis of SARS-CoV-2 [57]. It is
425 tempting to speculate that, similar to influenza virus, the SARS-CoV-2-induced pro-inflammatory state

426 may induce endothelial cells to express tissue factor, which in turn induces a pro-coagulant state,
427 microvascular leakage and pulmonary haemorrhage [58], all of which have been described in patients with
428 severe COVID-19. Furthermore, regardless of direct or indirect infection, elevated IL-6 correlates with
429 increased fibrinogen [59] and although still controversial, elevated fibrinogen levels have been detected
430 in critically ill patients [2].
431
432 The present study was subject to several limitations. Firstly, coagulation, thrombosis and induction of
433 angiogenesis in the lungs of deceased COVID-19 patients has been described in addition to endothelial
434 dysfunction [3]. This angiogenic response is thought to be predominantly mediated through
435 intussusceptive angiogenesis, where a new blood vessel is formed by splitting of an existing vessel.
436 This effect appears to be specific to COVID-19 patients, as lungs from decreased influenza patients do
437 not display increased angiogenic features. Whether this is due to relative hypoxia in the lungs remains
438 unclear, although elevated angiogenic growth factors such as VEGF-A and VEGF-C have been
439 associated with COVID-19 [3, 44]. In this study we have not addressed the effect of SARS-CoV-2 exposure
440 on the angiogenic capacity of endothelial cells in culture. Given the intimate association between
441 inflammation, endothelial dysfunction and angiogenesis [45, 60], these are critical aspects of COVID-19
442 pathology that remain to be addressed in subsequent studies. Similarly, due to the very low levels of
443 ACE2 present on endothelial cells it was not possible to determine if this was more pronounced on the
444 apical or basolateral surface of the endothelial cell.
445
446 An additional limitation of the present study is that, due to the reductionist nature of the *in vitro* systems
447 used herein, we were unable to address the contribution of immune cells to endothelial cell dysfunction
448 during SARS-CoV-2 infection. Multiple studies attribute the sustained inflammatory response directly
449 to immune cells, wherein macrophage activation, monocyte NLRP3 inflammasome signalling,
450 complement activation and extrusion of neutrophil extracellular traps are implicated [46, 61-63].
451 Accordingly, our data may best reflect the initial stages of infection when only a limited number of
452 tissue-resident leukocytes may be present. Future studies will necessitate the addition of leukocytes to

our co-culture system, to determine whether their presence results in a further induction of inflammation and markers of severe disease.

Here, we have conclusively shown that *in vitro,* endothelial cells are not productively infected by SARS-CoV-2 but that they mount an inflammatory response after direct or indirect exposure to the virus, characterised by increased cytokine secretion and expression of adhesion molecules. Our results thus suggest a key role of the endothelium in the pathogenesis of COVID-19, and that targeting the inflammatory response may present the best opportunity to prevent endothelial dysfunction.

ACKNOWLEDGEMENTS AND FUNDING STATEMENT

We thank Dr. Fernando Guimaraes for assisting with acquiring samples necessary for this study. This work is supported by the National Health and Medical Research Council of Australia (Fellowship 1141131 to KS, Fellowship 1124162 to LL, Project Grant APP1158002 to EG) and the Australian Research Council (Fellowship DE180100512 to KRS, Fellowship DE170100167 to EG, Discovery Project DP200100737 to EG and AL), The National Heart Foundation of Australia (Future Leader Fellowship 104692 to EG) and UQ Early Career Researcher Grants (UQECR2058733 to LS, UQECR2058045 to LL). Imaging was performed in IMB Microscopy incorporating the Cancer Ultrastructure and Function Facility funded by the Australian Cancer Research Foundation.

CONFLICT STATEMENT

KS is a co-inventor on patent applications for NLRP3 inhibitors which have been licensed to Inflazome Ltd, a company headquartered in Dublin, Ireland. Inflazome is developing drugs that target the NLRP3 inflammasome to address unmet clinical needs in inflammatory disease. KS served on the Scientific Advisory Board of Inflazome in 2016–2017, and serves as a consultant to Quench Bio, USA and Novartis, Switzerland.

DATA AVAILABILITY STATEMENT

All raw data is available upon request.

481

482 **REFERENCES**

483 1. Teuwen LA, Geldhof V, Pasut A, Carmeliet P. COVID-19: the vasculature unleashed. *Nat Rev*
484 *Immunol* 2020; **20**: 389-391.

485 2. Gu SX, Tyagi T, Jain K*, et al.* Thrombocytopathy and endotheliopathy: crucial contributors to
486 COVID-19 thromboinflammation. *Nature Reviews Cardiology* 2020.

487 3. Ackermann M, Verleden SE, Kuehnel M*, et al.* Pulmonary Vascular Endothelialitis,
488 Thrombosis, and Angiogenesis in Covid-19. *N Engl J Med* 2020; **383**: 120-128.

489 4. Goshua G, Pine AB, Meizlish ML*, et al.* Endotheliopathy in COVID-19-associated
490 coagulopathy: evidence from a single-centre, cross-sectional study. *Lancet Haematol* 2020; **7**:
491 e575-e582.

492 5. Sardu C, Gambardella J, Morelli MB, Wang X, Marfella R, Santulli G. Hypertension,
493 Thrombosis, Kidney Failure, and Diabetes: Is COVID-19 an Endothelial Disease? A
494 Comprehensive Evaluation of Clinical and Basic Evidence. *J Clin Med* 2020; **9**.

495 6. Gupta A, Madhavan MV, Sehgal K*, et al.* Extrapulmonary manifestations of COVID-19.
496 *Nature medicine* 2020; **26**: 1017-1032.

497 7. Cantuti-Castelvetri L, Ojha R, Pedro LD*, et al.* Neuropilin-1 facilitates SARS-CoV-2 cell entry
498 and infectivity. *Science* 2020.

499 8. Daly JL, Simonetti B, Klein K*, et al.* Neuropilin-1 is a host factor for SARS-CoV-2 infection.
500 *Science* 2020.

501 9. Zhou P, Yang X-L, Wang X-G*, et al.* A pneumonia outbreak associated with a new coronavirus
502 of probable bat origin. *Nature* 2020; **579**: 270-273.

503 10. Matheson NJ, Lehner PJ. How does SARS-CoV-2 cause COVID-19? *Science* 2020; **369**: 510-
504 511.

505 11. Hoffmann M, Kleine-Weber H, Schroeder S*, et al.* SARS-CoV-2 Cell Entry Depends on ACE2
506 and TMPRSS2 and Is Blocked by a Clinically Proven Protease Inhibitor. *Cell* 2020; **181**: 271-
507 280.e278.

508 12. Laporte M, Stevaert A, Raeymaekers V*, et al.* The SARS-CoV-2 and other human coronavirus
509 spike proteins are fine-tuned towards temperature and proteases of the human airways. *bioRxiv*
510 2020: 2020.2011.2009.374603.
511 13. Ferrario CM, Jessup J, Chappell MC*, et al.* Effect of angiotensin-converting enzyme inhibition
512 and angiotensin II receptor blockers on cardiac angiotensin-converting enzyme 2. *Circulation*
513 2005; **111**: 2605-2610.
514 14. Nicin L, Abplanalp WT, Mellentin H*, et al.* Cell type-specific expression of the putative SARS-
515 CoV-2 receptor ACE2 in human hearts. *Eur Heart J* 2020; **41**: 1804-1806.
516 15. Sluimer JC, Gasc JM, Hamming I*, et al.* Angiotensin-converting enzyme 2 (ACE2) expression
517 and activity in human carotid atherosclerotic lesions. *J Pathol* 2008; **215**: 273-279.
518 16. Lu R, Zhao X, Li J*, et al.* Genomic characterisation and epidemiology of 2019 novel
519 coronavirus: implications for virus origins and receptor binding. *Lancet* 2020; **395**: 565-574.
520 17. Hikmet F, Méar L, Edvinsson Å, Micke P, Uhlén M, Lindskog C. The protein expression profile
521 of ACE2 in human tissues. *Molecular Systems Biology* 2020; **16**: e9610.
522 18. Soker S, Takashima S, Miao HQ, Neufeld G, Klagsbrun M. Neuropilin-1 is expressed by
523 endothelial and tumor cells as an isoform-specific receptor for vascular endothelial growth
524 factor. *Cell* 1998; **92**: 735-745.
525 19. Kitsukawa T, Shimono A, Kawakami A, Kondoh H, Fujisawa H. Overexpression of a
526 membrane protein, neuropilin, in chimeric mice causes anomalies in the cardiovascular system,
527 nervous system and limbs. *Development* 1995; **121**: 4309-4318.
528 20. Gerhardt H, Ruhrberg C, Abramsson A, Fujisawa H, Shima D, Betsholtz C. Neuropilin-1 is
529 required for endothelial tip cell guidance in the developing central nervous system.
530 *Developmental dynamics : an official publication of the American Association of Anatomists*
531 2004; **231**: 503-509.
532 21. Jones EA, Yuan L, Breant C, Watts RJ, Eichmann A. Separating genetic and hemodynamic
533 defects in neuropilin 1 knockout embryos. *Development* 2008; **135**: 2479-2488.
534 22. Aspalter IM, Gordon E, Dubrac A*, et al.* Alk1 and Alk5 inhibition by Nrp1 controls vascular
535 sprouting downstream of Notch. *Nature communications* 2015; **6**.

536 23. Aimes RT, Zijlstra A, Hooper JD, *et al.* Endothelial cell serine proteases expressed during
537 vascular morphogenesis and angiogenesis. *Thromb Haemost* 2003; **89**: 561-572.
538 24. Chen L, Li X, Chen M, Feng Y, Xiong C. The ACE2 expression in human heart indicates new
539 potential mechanism of heart injury among patients infected with SARS-CoV-2.
540 *Cardiovascular research* 2020; **116**: 1097-1100.
541 25. McCracken IR, Saginc G, He L, *et al.* Lack of Evidence of Angiotensin-Converting Enzyme 2
542 Expression and Replicative Infection by SARS-CoV-2 in Human Endothelial Cells. *Circulation*
543 2021; **143**: 865-868.
544 26. Fosse JH, Haraldsen G, Falk K, Edelmann R. Endothelial Cells in Emerging Viral Infections.
545 *Frontiers in Cardiovascular Medicine* (Review).2021; **8**.
546 27. Bryce C, Grimes Z, Pujadas E, *et al.* Pathophysiology of SARS-CoV-2: targeting of endothelial
547 cells renders a complex disease with thrombotic microangiopathy and aberrant immune
548 response. The Mount Sinai COVID-19 autopsy experience. *medRxiv* 2020:
549 2020.2005.2018.20099960.
550 28. Schaefer I-M, Padera RF, Solomon IH, *et al.* In situ detection of SARS-CoV-2 in lungs and
551 airways of patients with COVID-19. *Modern Pathology* 2020; **33**: 2104-2114.
552 29. Varga Z, Flammer AJ, Steiger P, *et al.* Endothelial cell infection and endotheliitis in COVID-
553 19. *Lancet* 2020; **395**: 1417-1418.
554 30. Amraie R, Napoleon MA, Yin W, *et al.* CD209L/L-SIGN and CD209/DC-SIGN act as
555 receptors for SARS-CoV-2 and are differentially expressed in lung and kidney epithelial and
556 endothelial cells. *bioRxiv* 2020: 2020.2006.2022.165803.
557 31. Wang P, Luo R, Zhang M, *et al.* A cross-talk between epithelium and endothelium mediates
558 human alveolar–capillary injury during SARS-CoV-2 infection. *Cell Death & Disease* 2020;
559 **11**: 1042.
560 32. Monteil V, Kwon H, Prado P, *et al.* Inhibition of SARS-CoV-2 Infections in Engineered Human
561 Tissues Using Clinical-Grade Soluble Human ACE2. *Cell* 2020; **181**: 905-913.e907.
562 33. Delorey TM, Ziegler CGK, Heimberg G, *et al.* A single-cell and spatial atlas of autopsy tissues
563 reveals pathology and cellular targets of SARS-CoV-2. *bioRxiv* 2021: 2021.2002.2025.430130.

564 34. Ko CJ, Harigopal M, Gehlhausen JR, Bosenberg M, McNiff JM, Damsky W. Discordant anti-
565 SARS-CoV-2 spike protein and RNA staining in cutaneous perniotic lesions suggests
566 endothelial deposition of cleaved spike protein. *Journal of Cutaneous Pathology* **n/a**.
567 35. Baeck M, Hoton D, Marot L, Herman A. Chilblains and COVID-19: why SARS-CoV-2
568 endothelial infection is questioned. *British Journal of Dermatology* **n/a**.
569 36. Sia SF, Yan L-M, Chin AWH*, et al.* Pathogenesis and transmission of SARS-CoV-2 in golden
570 hamsters. *Nature* 2020; **583**: 834-838.
571 37. Rockx B, Kuiken T, Herfst S*, et al.* Comparative pathogenesis of COVID-19, MERS, and
572 SARS in a nonhuman primate model. *Science* 2020; **368**: 1012-1015.
573 38. Aid M, Busman-Sahay K, Vidal SJ*, et al.* Vascular Disease and Thrombosis in SARS-CoV-2-
574 Infected Rhesus Macaques. *Cell* 2020; **183**: 1354-1366.e1313.
575 39. Milewska A, Kula-Pacurar A, Wadas J*, et al.* Replication of Severe Acute Respiratory
576 Syndrome Coronavirus 2 in Human Respiratory Epithelium. *Journal of Virology* 2020; **94**:
577 e00957-00920.
578 40. Andersson MI, Arancibia-Carcamo CV, Auckland K*, et al.* SARS-CoV-2 RNA detected in
579 blood products from patients with COVID-19 is not associated with infectious virus. *Wellcome*
580 *Open Res* 2020; **5**: 181.
581 41. Gordon DE, Jang GM, Bouhaddou M*, et al.* A SARS-CoV-2 protein interaction map reveals
582 targets for drug repurposing. *Nature* 2020; **583**: 459-468.
583 42. Polacheck WJ, Kutys ML, Tefft JB, Chen CS. Microfabricated blood vessels for modeling the
584 vascular transport barrier. *Nat Protoc* 2019; **14**: 1425-1454.
585 43. Conceicao C, Thakur N, Human S*, et al.* The SARS-CoV-2 Spike protein has a broad tropism
586 for mammalian ACE2 proteins. *PLOS Biology* 2020; **18**: e3001016.
587 44. Lucas C, Wong P, Klein J*, et al.* Longitudinal analyses reveal immunological misfiring in
588 severe COVID-19. *Nature* 2020; **584**: 463-469.
589 45. Pober JS, Sessa WC. Evolving functions of endothelial cells in inflammation. *Nat Rev Immunol*
590 2007; **7**: 803-815.

591 46. Rodrigues TS, de Sá KSG, Ishimoto AY, *et al.* Inflammasomes are activated in response to
592 SARS-CoV-2 infection and are associated with COVID-19 severity in patients. *Journal of*
593 *Experimental Medicine* 2020; **218**.
594 47. Kasper J, Hermanns MI, Bantz C, *et al.* Inflammatory and cytotoxic responses of an alveolar-
595 capillary coculture model to silica nanoparticles: Comparison with conventional monocultures.
596 *Particle and Fibre Toxicology* 2011; **8**: 6.
597 48. Kummer S, Avinoam O, Kräusslich H-G. IFITM3 Clusters on Virus Containing Endosomes
598 and Lysosomes Early in the Influenza A Infection of Human Airway Epithelial Cells. *Viruses*
599 2019; **11**: 548.
600 49. Winstone H, Lista MJ, Reid A, *et al.* The polybasic cleavage site in the SARS-CoV-2 spike
601 modulates viral sensitivity to Type I IFN and IFITM2. *bioRxiv* 2020: 2020.2012.2019.423592.
602 50. Buzhdygan TP, DeOre BJ, Baldwin-Leclair A, *et al.* The SARS-CoV-2 spike protein alters
603 barrier function in 2D static and 3D microfluidic in vitro models of the human blood-brain
604 barrier. *bioRxiv* 2020: 2020.2006.2015.150912.
605 51. Bradley BT, Maioli H, Johnston R, *et al.* Histopathology and ultrastructural findings of fatal
606 COVID-19 infections in Washington State: a case series. *Lancet* 2020; **396**: 320-332.
607 52. Manne BK, Denorme F, Middleton EA, *et al.* Platelet gene expression and function in patients
608 with COVID-19. *Blood* 2020; **136**: 1317-1329.
609 53. Schurink B, Roos E, Radonic T, *et al.* Viral presence and immunopathology in patients with
610 lethal COVID-19: a prospective autopsy cohort study. *Lancet Microbe* 2020; **1**: e290-e299.
611 54. Meizlish M, Pine A, Goshua G, *et al.* Circulating Markers of Angiogenesis and
612 Endotheliopathy in COVID-19. *medRxiv* 2020: 2020.2006.2029.20140376.
613 55. Bost P, Giladi A, Liu Y, *et al.* Host-Viral Infection Maps Reveal Signatures of Severe COVID-
614 19 Patients. *Cell* 2020; **181**: 1475-1488.e1412.
615 56. Short KR, Kasper J, van der Aa S, *et al.* Influenza virus damages the alveolar barrier by
616 disrupting epithelial cell tight junctions. *Eur Respir J* 2016; **47**: 954-966.
617 57. Bernard I, Limonta D, Mahal LK, Hobman TC. Endothelium Infection and Dysregulation by
618 SARS-CoV-2: Evidence and Caveats in COVID-19. *Viruses* 2020; **13**.

619 58. Goeijenbier M, van Gorp ECM, Van den Brand JMA*, et al.* Activation of coagulation and tissue
620 fibrin deposition in experimental influenza in ferrets. *BMC Microbiology* 2014; **14**: 134.
621 59. Ranucci M, Ballotta A, Di Dedda U*, et al.* The procoagulant pattern of patients with COVID-
622 19 acute respiratory distress syndrome. *J Thromb Haemost* 2020; **18**: 1747-1751.
623 60. McDonald DM, Yao LC, Baluk P. Dynamics of airway blood vessels and lymphatics: lessons
624 from development and inflammation. *Proc Am Thorac Soc* 2011; **8**: 504-507.
625 61. Merad M, Martin JC. Pathological inflammation in patients with COVID-19: a key role for
626 monocytes and macrophages. *Nat Rev Immunol* 2020; **20**: 355-362.
627 62. Middleton EA, He XY, Denorme F*, et al.* Neutrophil extracellular traps contribute to
628 immunothrombosis in COVID-19 acute respiratory distress syndrome. *Blood* 2020; **136**: 1169-
629 1179.
630 63. Zuo Y, Yalavarthi S, Shi H*, et al.* Neutrophil extracellular traps in COVID-19. *JCI Insight*
631 2020; **5**.

632

633

634 **FIGURE LEGENDS**

635 **Figure 1. In vivo sections of lung show endothelial cells are not infected.** Lung tissue from 4
636 deceased COVID-19 patients was sectioned and stained for Hematoxylin and Eosin
637 (H&E)(0). Consecutive sections were stained using RNAscope probes targeting either SARS-CoV-
638 2 spike mRNA or negative control probe and Syto13 for DNA. Patients 1 and 2 are positive for SARS-
639 CoV-2 spike mRNA (enlargement 1 and 2). Further enlargements of numbered insets (3-6) show vessels
640 outlined with red dashed line are negative for SARS-CoV-2 spike mRNA in the endothelial layer of the
641 vessels. Negative control probe shows non-specific background staining.

642

643 **Figure 2. Endothelial cells express very low levels of ACE2 and TMPRSS2 receptors. A)** qPCR
644 shows presence of mRNA for ACE2, TMPRSS2 and NRP1 in HUVEC, HMVEC-L and Calu-3 cells.
645 n=3 independent experiments. **B)** Representative immunofluorescent images of HUVEC, HMVEC-L
646 and Calu-3 cells stained for ACE2 (shown as single channel in top panel) (green), Phalloidin (magenta)
647 and DAPI (blue). Scalebar 30 µm. **C)** Quantification of ACE2 staining intensity. n=15 images; 5 images
648 per independent experiments. **D)** Western blot analysis showing ACE2 protein levels are absent in
649 negative control BHK-21 cells, lower in HUVEC and HMVEC-L compared to Calu-3 cells and
650 HUVEC + ACE2 overexpression and Human Nasal Epithelium cells (HNEp) as positive controls in top
651 panel. TMPRSS2 protein levels are lower in HUVEC and HMVEC-L compared to Calu-3 cells in
652 bottom panel **E)** Quantification of protein levels for ACE2 and TMPRSS2 in HUVEC, HMVEC-L and
653 Calu-3. n=5 (HUVEC and HMVEC-L), n=3 (Calu-3) independent experiments. **D)** Data are presented
654 as mean±s.e.m. with individual data points indicated and colour coded per independent experimental
655 replicate. Statistical significance was determined using a Kruskal Wallis test between Calu-3 and all
656 others (A, C, E). *P<0.05, ****P<0.0001.

657

658 **Figure 3. Endothelial cells can be infected with 2 x 10^6 PFU of SARS-CoV-2, but infection is**
659 **abortive. A)** Viral replication shown as number of PFU per ml of supernatant from SARS-CoV-2
660 infected HUVEC, HMVEC-L and Calu-3 cells at 24h, 48h and 72h after infection. n=2 (HUVEC and
661 HMVEC-L), n=3 (Calu-3) independent experiments. **B)** Representative immunofluorescent images of

662 HMVEC-L stained for NP (shown as single channel in top panel) (green), phalloidin (magenta) and
663 DAPI (blue) with mock or SARS-CoV-2 infection from either apical or basolateral side of the cells at
664 72h after infection. Scalebar 50 µm. **B')** Enlargement of white box in B shows Phalloidin and DAPI
665 single channels and merge. Scalebar 10 µm. **B'')** XZ projection of merged image in B', with apical side
666 on top of image and basolateral side on the bottom. Scalebar 10 µm. **C)** Quantification of NP staining
667 intensity in HMVEC-L. n=15 images from 3 independent experiments. **D)** Quantification of % NP
668 positive cells that are extruded upon SARS-CoV-2 infection of HMVEC-Ls. n=15 images from 3
669 independent experiments. **E)** Western blot analysis showing NP protein levels in HUVEC, HMVEC-L
670 and Calu-3 cells after 72h of infection. **F)** Quantification of NP protein levels in HUVEC, HMVEC-L
671 and Calu-3. n=3 independent experiments. **G)** Representative immunofluorescent images of HMVEC-
672 L and Calu-3 stained for NP (shown as single channel in top left panel) (green), cleaved caspase 3 (CC
673 3) (shown as single channel in top right panel)(magenta) and DAPI (blue) with mock or SARS-CoV-2
674 infection from apical side of the cells at 72h after infection. Scalebar 50 µm. **H)** Quantification of %
675 NP positive cells that are positive for apoptosis marker cleaved caspase 3. n=15 images from 3
676 independent experiments. Data are presented as mean±s.e.m. with individual data points indicated and
677 colour coded per independent experimental replicate. Statistical significance was determined using
678 Kruskal Wallis test between 24h and other time points (A) or Mann-Whitney test between mock and +
679 SARS-CoV-2 (C, F, H). *P<0.05, ***P<0.001, ****P<0.0001.
680
681 **Figure 4. Endothelial cells are not infected with 2 x 10^6 PFU of SARS-CoV-2 in 3D. A)** Schematic
682 of microfabricated device used to culture 3D vessel tubes under oscillatory flow. Cross section shows
683 luminized tube covered with endothelial cells surrounded by extracellular matrix and virus can be
684 flowed through the lumen of those tubes. **B)** Viral replication shown as number of PFU per ml of
685 supernatant from SARS-CoV-2 infected HMVEC-L and Vero cells at 24h after infection. n=3
686 (HMVEC-L), n=2 (Ver0) independent experiments. Representative immunofluorescent images of **C)**
687 HMVEC-L and **D)** Vero stained for NP (shown as single channel in top panel) (green), phalloidin
688 (magenta) and DAPI (blue) with mock or SARS-CoV-2 infection in the lumen of the tube at 24h after
689 infection. Scalebar 50 µm. YZ projection of **E)** HMVEC-L (merged image in C) and **F)** Vero (merged

690 image in D), with luminal side towards the right of image and basolateral side towards the right of
691 images. Scalebar 20 µm.
692
693 **Figure 5. Endothelial cells mount an inflammatory response upon infection.** Representative
694 immunofluorescent images of HMVEC-L stained for ICAM-1 (shown as single channel in top panel)
695 (green), NP (magenta), phalloidin (grey) and DAPI (blue) with **A)** mock or SARS-CoV-2 infection
696 from either apical or basolateral side of the cells at 72h after infection or with **B)** control and TNFα
697 treatment for 72h. Scalebar 50 µm. **C)** Quantification of ICAM-1 staining intensity in HMVEC-L. n=15
698 images from 3 independent experiments. **D)** Western blot analysis showing ICAM-1 and NP protein
699 levels in HMVEC-L and Calu-3 cells after 72h of infection. **E)** Quantification of ICAM-1 protein levels
700 in HMVEC-L and Calu-3. n=3 independent experiments. Measurement of cytokines with AlphaLISA
701 Immunoassay kit for **F)** CXCL10 and **G)** IL6 in the supernatant of HMVEC-L with mock or SARS-
702 CoV-2 infection from either apical or basolateral side of the cells at 72h after infection. n=4 independent
703 experiments. Data are presented as mean±s.e.m. with individual data points indicated and colour coded
704 per independent experimental replicate. Statistical significance was determined using Mann-Whitney
705 test between mock and + SARS-CoV-2 (C, E, F, G). *P<0.05, ****P<0.0001.
706
707 **Figure 6. Co-culture shows infection of Calu-3 and inflammation of HMVEC-L. A)** Representative
708 immunofluorescent images of co-cultured Calu-3 and HMVEC-L stained for NP (shown as single
709 channel in top panel) (magenta), ICAM-1 (shown as single channel in middle panel) (green), phalloidin
710 (grey) and DAPI (blue) with mock or SARS-CoV-2 infection at 72h after infection (2 x 10^6 PFU).
711 Scalebar 50 µm. **B)** Quantification of NP staining intensity in Calu-3 and HMVEC-L. n=9 images from
712 3 independent experiments. **C)** Schematic of Calu-3 and HMVEC-L co-cultures on transwell
713 membranes. **D)** Quantification of ICAM-1 staining intensity in Calu-3 and HMVEC-L. n=9 images
714 from 3 independent experiments. **E)** Representative immunofluorescent images of co-cultured Calu-3
715 and HMVEC-L stained for dsRNA (shown as single channel in top panel) (magenta), phalloidin (grey)
716 and DAPI (blue) with mock or SARS-CoV-2 infection at 72h after infection. Scalebar 50 µm. **F)**
717 Quantification of dsRNA staining intensity in Calu-3 and HMVEC-L. n=9 images from 3 independent

718 experiments. **G)** qPCR shows presence of viral RNA (MPRO) in SARS-CoV-2 infected Calu-3 and
719 HMVEC-L co-cultured cells represented as fold change relative to mock infection at 72h after infection.
720 n=3 independent experiments. **H)** Viral replication shown as number of PFU per ml of supernatant from
721 SARS-CoV-2 infected Calu-3 and HMVEC-L co-cultured cells at 72h after infection. n=3 independent
722 experiments. Measurement of cytokines with AlphaLISA Immunoassay kit for **I)** CXCL10 and **J)** IL6
723 in the supernatant of Calu-3 and HMVEC-L co-cultured cells with mock or SARS-CoV-2 infection at
724 72h after infection. n=4 independent experiments. Data are presented as mean±s.e.m. with individual
725 data points indicated and colour coded per independent experimental replicate. Statistical significance
726 was determined using Mann-Whitney test between mock and + SARS-CoV-2 (B, D, F, G, H, I, J).
727 *P<0.05, **P<0.01, ****P<0.0001.
728
729 **Supplemental Table 1. Patient information.** Additional information on cohort of COVID-19 patients.
730
731 **Supplemental Figure 1. Endothelial cells are not productively infected with 6 x 10^4 PFU of SARS-**
732 **CoV-2.** Schematic of **A)** apical and **B)** basolateral infection of cells cultured on transwell membranes.
733 **C)** Viral replication shown as number of PFU per ml of supernatant from SARS-CoV-2 infected
734 HUVEC, HMVEC-L and Calu-3 cells at 24h, 48h and 72h after infection. n=2 (HUVEC and HMVEC-
735 L), n=3 (Calu-3) independent experiments. Representative immunofluorescent images of **D)** HUVEC,
736 **E)** Calu-3 or **F)** HMVEC-L stained for NP (shown as single channel in top panel) (green), phalloidin
737 (magenta) and DAPI (blue) with mock or SARS-CoV-2 infection from either apical or basolateral side
738 of the cells at 48h after infection. Scalebar 50 µm. **G)** Quantification of NP staining intensity in
739 HUVEC, HMVEC-L and Calu-3. n=9 images from 3 independent experiments. **H)** Western blot
740 analysis showing NP protein levels in HUVEC, HMVEC-L and Calu-3 cells after 48h of infection. **I)**
741 Quantification of protein levels for NP in HUVEC, HMVEC-L and Calu-3. n=2 independent
742 experiments. Data are presented as mean±s.e.m. with individual data points indicated and colour coded
743 per independent experimental replicate. Statistical significance was determined using Kruskal Wallis
744 test between 24h and other time points (C) or Mann-Whitney test between mock and + SARS-CoV-2
745 (G, I). *P<0.05, **P<0.01

746

747 **Supplemental Figure 2. Positive and negative controls for infection with 6 x 10^4 PFU of SARS-**
748 **CoV-2. A)** Viral replication shown as number of PFU per ml of supernatant from SARS-CoV-2 infected
749 BHK-2 and Calu-3 cells at 72h after infection. n=3 independent experiments. **B)** Western blot analysis
750 showing NP protein levels in BHK-21 and Calu-3 cells after 72h of apical infection with mock or SARS-
751 CoV-2. **C)** Quantification of protein levels for NP in BHK-21 and Calu-3. n=3 independent experiment.
752 **D)** Representative immunofluorescent images of BHK-21 and Calu-3 cells stained for NP (shown as
753 single channel in top panel) (green), phalloidin (magenta) and DAPI (blue) with mock or SARS-CoV-
754 2 infection from apical side of the cells at 72h after infection. Scalebar 50 µm. **E)** Quantification of NP
755 staining intensity in BHK-21 and Calu-3. n=9 images from 3 independent experiments. Maximum
756 secretion levels of **F)** CXCL10 and **G)** IL6 in the supernatant of HMVEC-L with mock, TNFα or IFNß
757 treatment from the apical side of the cells at 4h and 16h after treatment. n=2 independent experiments.
758 Data are presented as mean±s.e.m. with individual data points indicated and colour coded per
759 independent experimental replicate. Statistical significance was determined using Mann-Whitney test
760 between mock and + SARS-CoV-2 (C, E). ****P<0.0001

761

762 **Supplemental Figure 3. Full scans of Western blots.** Full scans of Western blots shown in the paper
763 figures. Used lanes are labelled as in the corresponding figure, with other lanes labelled as X. Dashed
764 line indicates where membrane was cut. Underlined proteins indicate which blot was used in the
765 corresponding figure and time indicates exposure time.

766

767

768

769

770

Figure 1

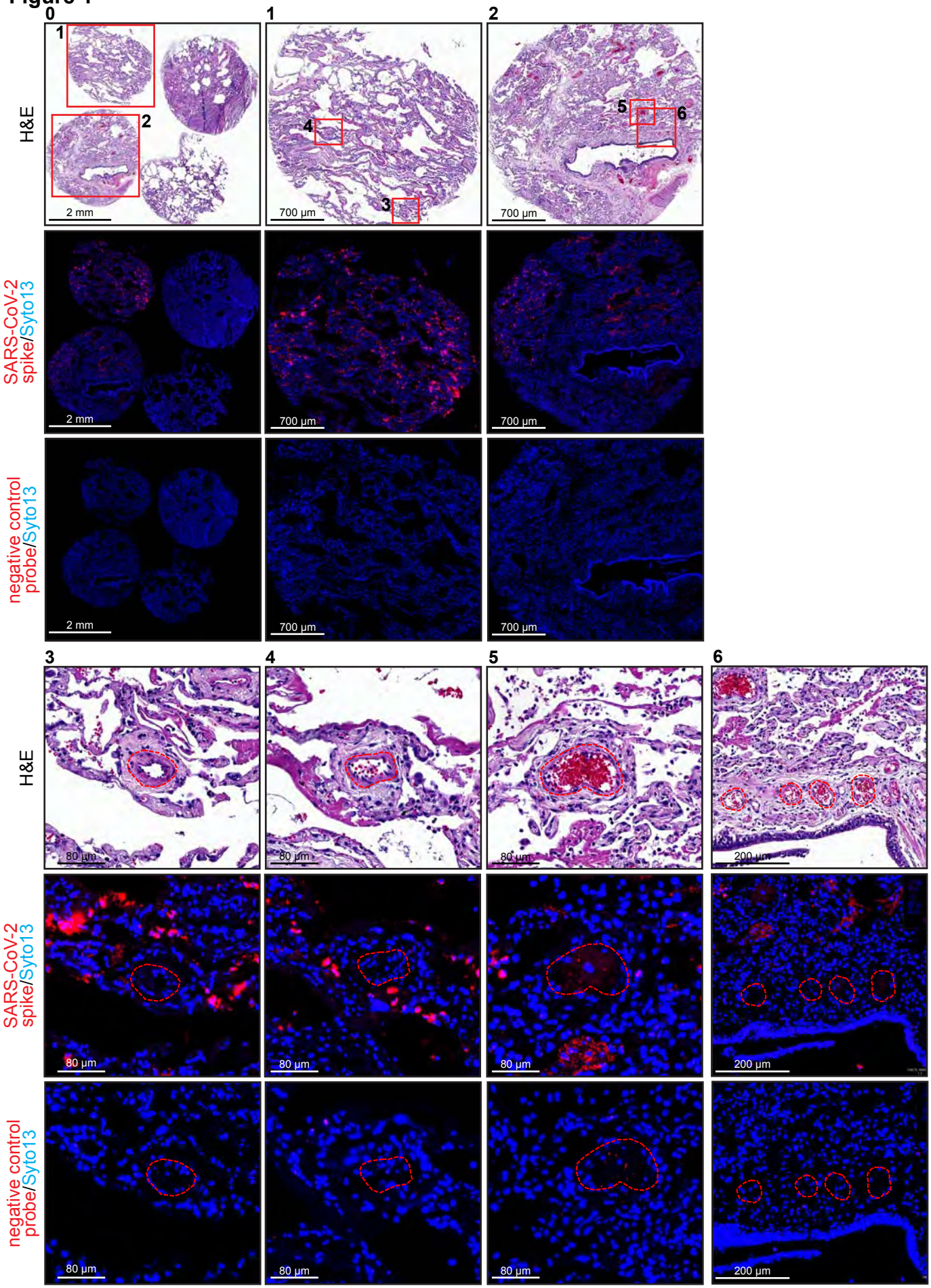
0
1
2
H&E
SARS-CoV-2 spike/Syto13
negative control probe/Syto13
2 mm
700 µm
3
4
5
6
80 µm
200 µm

Figure 2

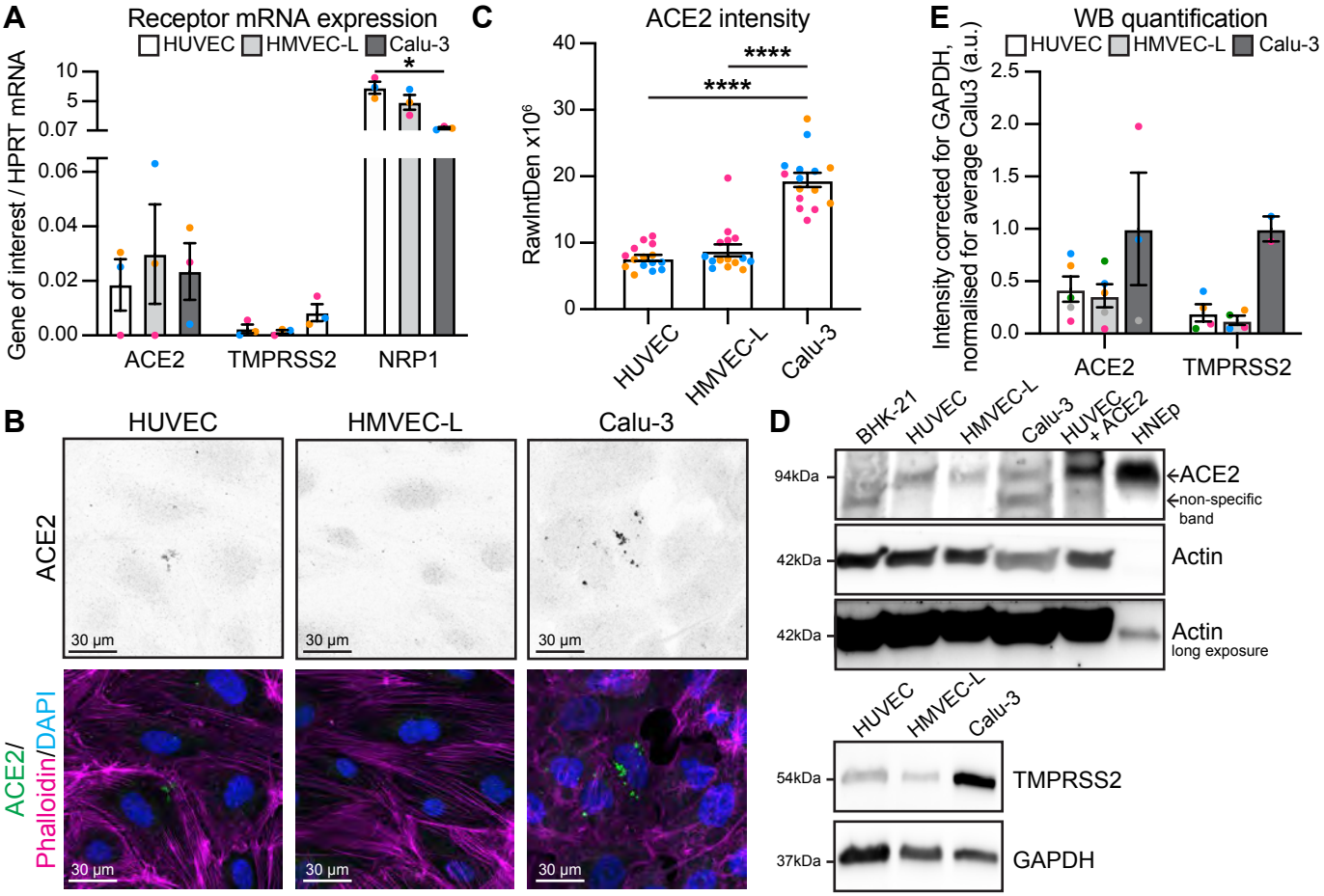
A
Receptor mRNA expression
HUVEC HMVEC-L Calu-3
Gene of interest / HPRT mRNA
10
5
0.07
0.06
0.04
0.02
0.00
*
ACE2
TMPRSS2
NRP1
C
ACE2 intensity
RawIntDen x10^6
40
30
20
10
0
****
****
HUVEC
HMVEC-L
Calu-3
E
WB quantification
HUVEC HMVEC-L Calu-3
Intensity corrected for GAPDH, normalised for average Calu3 (a.u.)
2.5
2.0
1.5
1.0
0.5
0.0
ACE2
TMPRSS2
B
HUVEC
HMVEC-L
Calu-3
ACE2
ACE2/ Phalloidin/DAPI
30 µm
D
BHK-21
HUVEC
HMVEC-L
Calu-3
HUVEC + ACE2
HNEp
94kDa
ACE2
non-specific band
42kDa
Actin
42kDa
Actin
long exposure
HUVEC
HMVEC-L
Calu-3
54kDa
TMPRSS2
37kDa
GAPDH

Figure 3

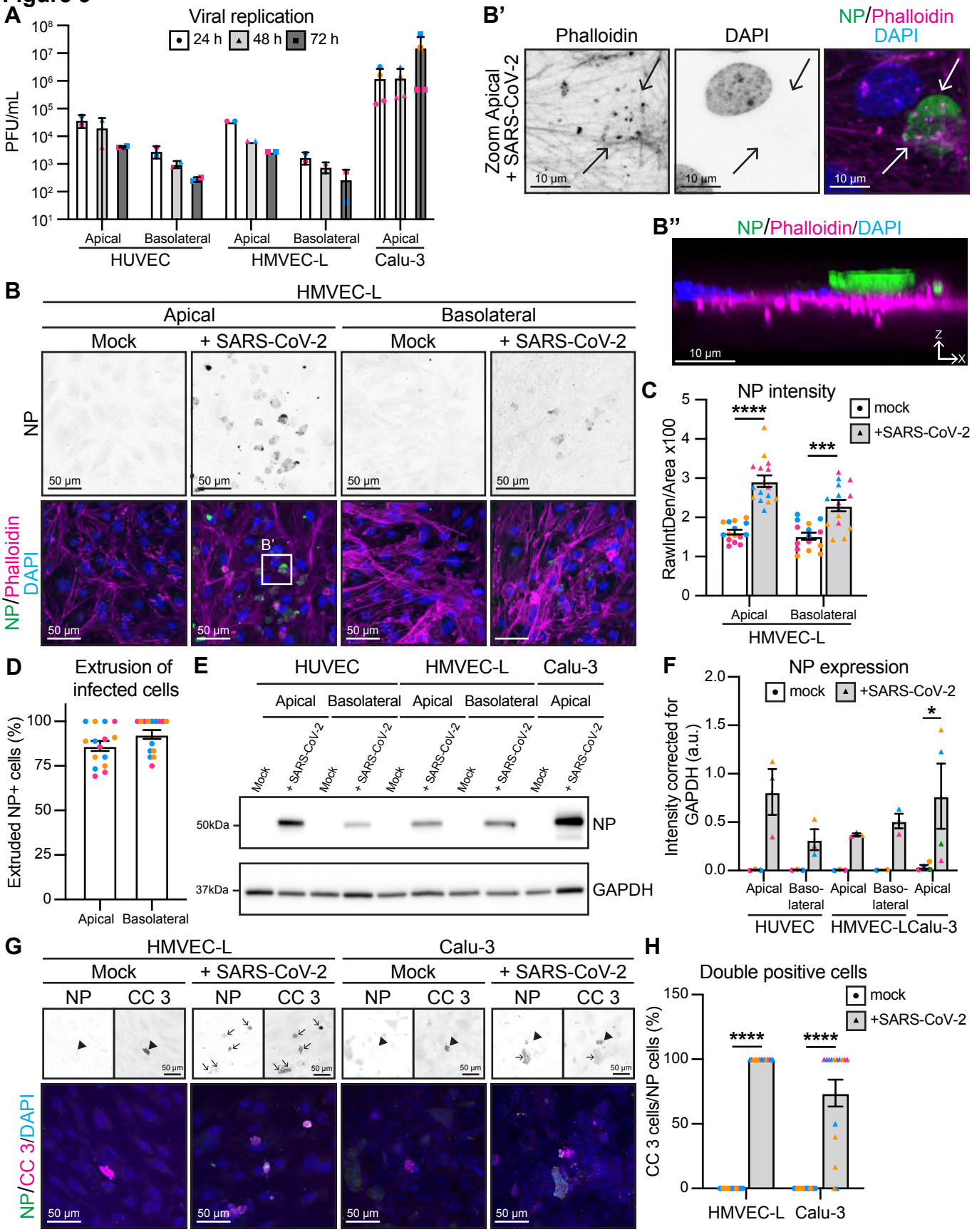
A
Viral replication
24 h
48 h
72 h
PFU/mL
Apical
Basolateral
HUVEC
HMVEC-L
Calu-3
B'
Phalloidin
DAPI
NP/Phalloidin
DAPI
Zoom Apical
+ SARS-CoV-2
10 µm
B''
NP/Phalloidin/DAPI
B
HMVEC-L
Apical
Basolateral
Mock
+ SARS-CoV-2
NP
NP/Phalloidin
DAPI
50 µm
C
NP intensity
mock
+SARS-CoV-2
RawIntDen/Area x100
****
***
D
Extrusion of
infected cells
Extruded NP+ cells (%)
E
HUVEC
HMVEC-L
Calu-3
50kDa
37kDa
NP
GAPDH
F
NP expression
Intensity corrected for
GAPDH (a.u.)
Baso-
lateral
G
CC 3
NP/CC 3/DAPI
H
Double positive cells
CC 3 cells/NP cells (%)

Figure 4

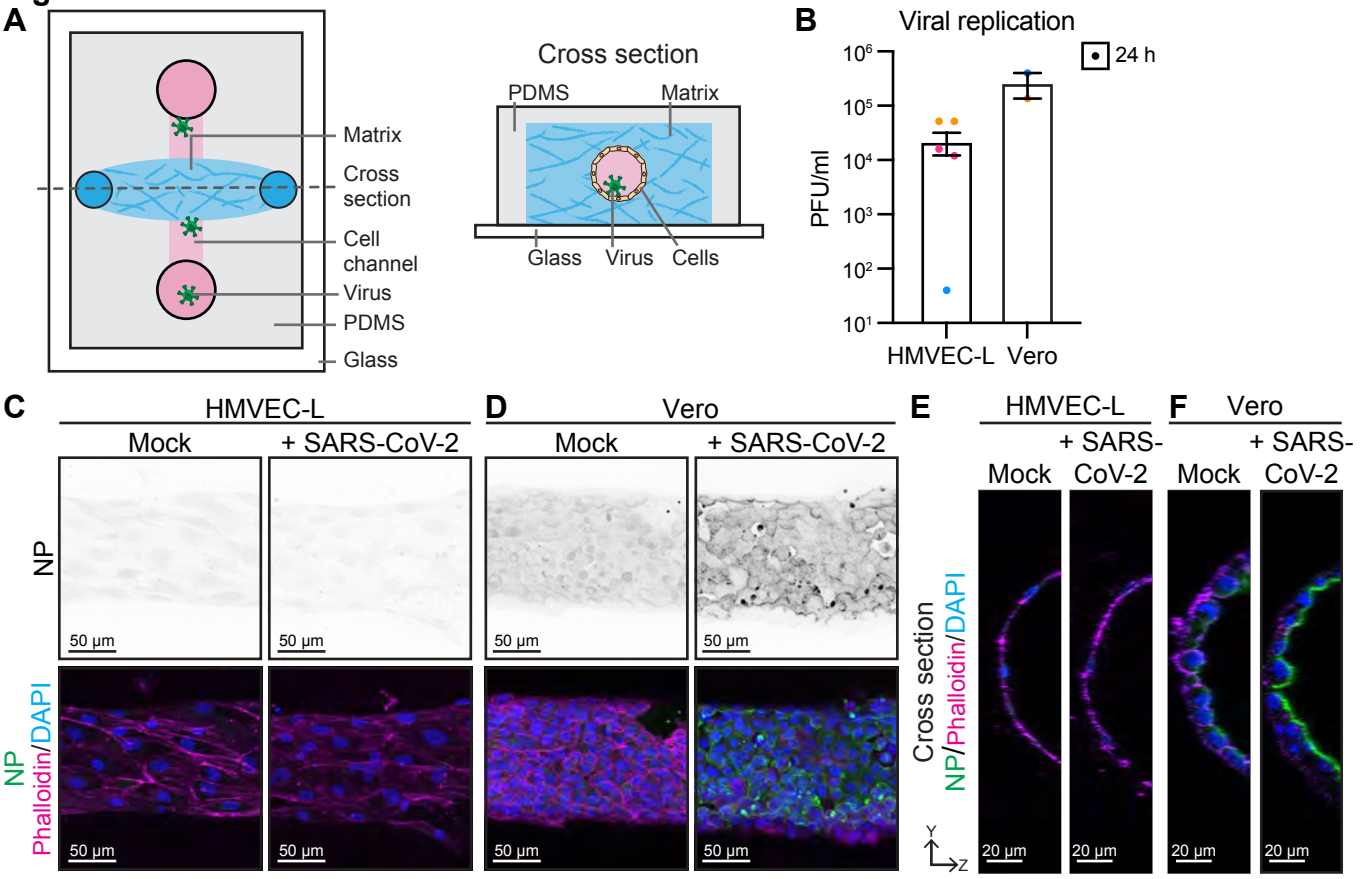
A
Matrix
Cross section
Cell channel
Virus
PDMS
Glass
Cross section
PDMS
Matrix
Glass
Virus
Cells
B
Viral replication
24 h
PFU/ml
10^6
10^5
10^4
10^3
10^2
10^1
HMVEC-L
Vero
C
HMVEC-L
Mock
+ SARS-CoV-2
NP
NP
Phalloidin/DAPI
50 µm
D
Vero
Mock
+ SARS-CoV-2
E
HMVEC-L
Mock
+ SARS-CoV-2
F
Vero
Mock
+ SARS-CoV-2
Cross section
NP/Phalloidin/DAPI
Y
Z
20 µm

Figure 5

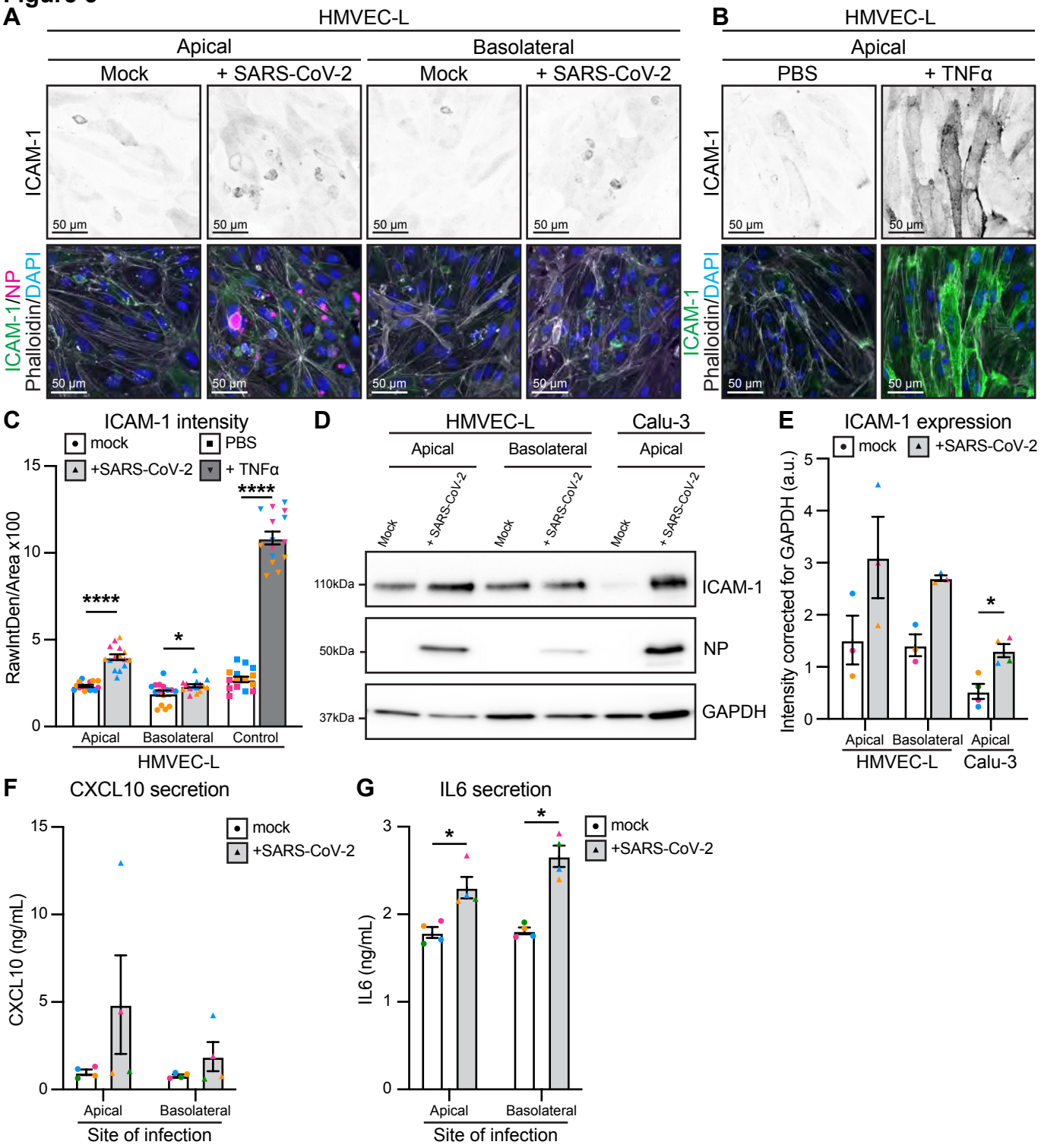
A
HMVEC-L
Apical
Basolateral
Mock
+ SARS-CoV-2
Mock
+ SARS-CoV-2
ICAM-1
ICAM-1/NP
Phalloidin/DAPI
50 µm
B
HMVEC-L
Apical
PBS
+ TNFα
ICAM-1
ICAM-1
Phalloidin/DAPI
C
ICAM-1 intensity
mock
PBS
+SARS-CoV-2
+ TNFα
RawIntDen/Area x100
****
*
****
Apical
Basolateral
Control
HMVEC-L
D
HMVEC-L
Calu-3
Apical
Basolateral
Apical
Mock
+ SARS-CoV-2
110kDa
50kDa
37kDa
ICAM-1
NP
GAPDH
E
ICAM-1 expression
mock
+SARS-CoV-2
Intensity corrected for GAPDH (a.u.)
*
Apical
Basolateral
Apical
HMVEC-L
Calu-3
F
CXCL10 secretion
mock
+SARS-CoV-2
CXCL10 (ng/mL)
Apical
Basolateral
Site of infection
G
IL6 secretion
mock
+SARS-CoV-2
IL6 (ng/mL)
*
*
Apical
Basolateral
Site of infection

Figure 6

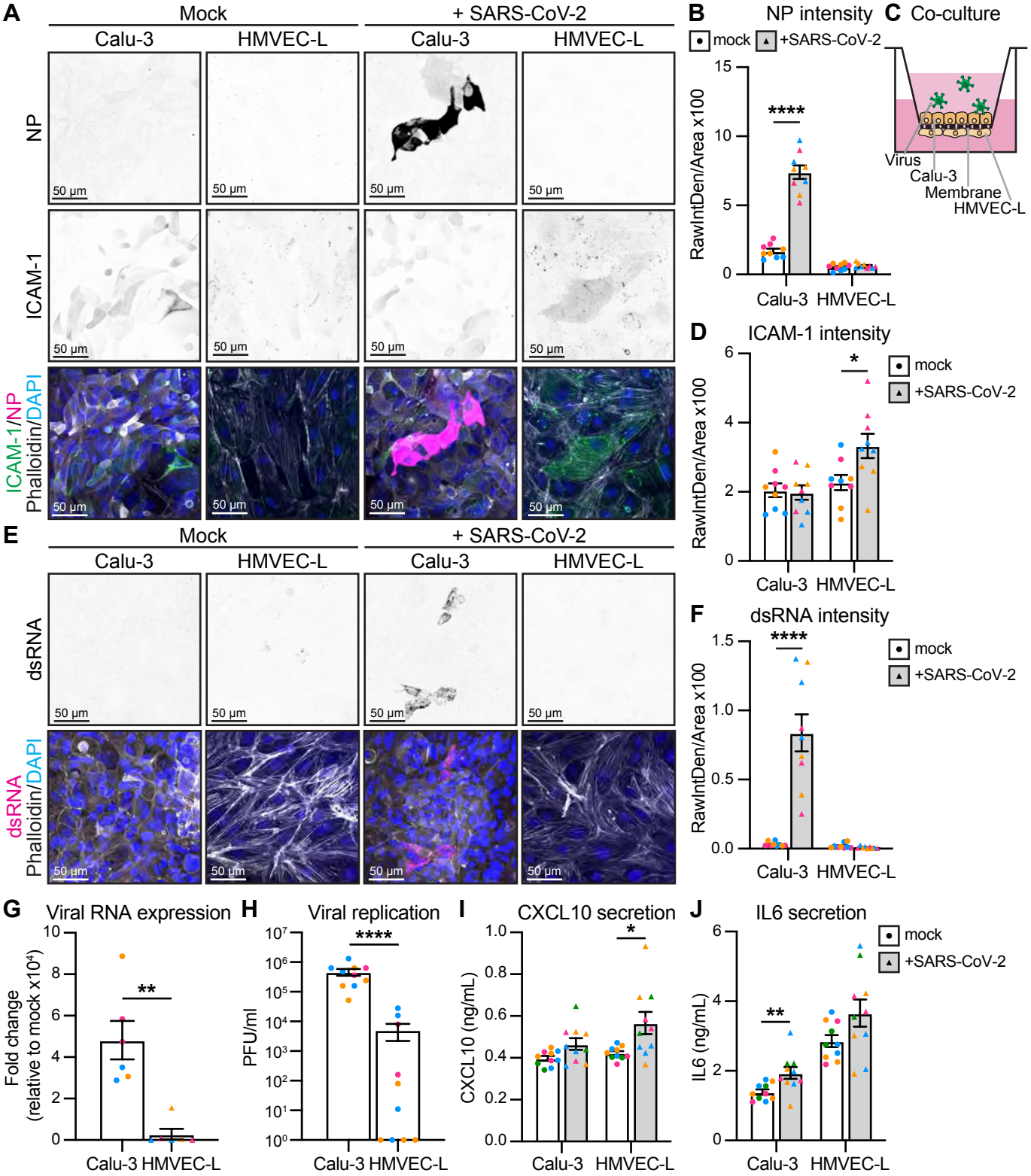
A
Mock
+ SARS-CoV-2
Calu-3
HMVEC-L
NP
ICAM-1
ICAM-1/NP
Phalloidin/DAPI
50 µm
B
NP intensity
mock
+SARS-CoV-2
RawIntDen/Area x100
****
C
Co-culture
Virus
Calu-3
Membrane
HMVEC-L
D
ICAM-1 intensity
*
E
dsRNA
dsRNA
Phalloidin/DAPI
F
dsRNA intensity
G
Viral RNA expression
Fold change
(relative to mock x10⁴)
**
H
Viral replication
PFU/ml
I
CXCL10 secretion
CXCL10 (ng/mL)
J
IL6 secretion
IL6 (ng/mL)

Supplemental Table 1: Patient information

*representative images derived from this patient

Patient ID	Diagnosis	Sex	Age	Co-morbidities	Histology	D-Dimer at admission
LN1*	COVID-19	F	87	Systemic Arterial Hypertension, Dyslipidemia, Hypothyroidism, Senile dementia	Acute phase DAD	2014
LN2	COVID-19	M	53	Class II obesity	Acute phase DAD	425
LN3	COVID-19	F	85	Systemic Arterial Hypertension, Brain Stroke, Vascular Dementia	Acute phase DAD	N/A
LN4	COVID-19	M	73	Type 2 Diabetes Mellitus, Chronic Kidney Disease Dialysis, Atrial Fibrillation, Coronary Disease, Heart Failure, Peripheral Obstructive Artery Disease	Reactive Type 2 pneumocyte hyplerplasia	3436
LN6	COVID-19	M	80	Systemic Arterial Hypertension, Coronary Disease, Heart Failure, Class III obesity	Reactive Type 2 pneumocyte hyplerplasia	816
LN7	COVID-19	M	81	Systemic Arterial Hypertension, Chronic Kidney Disease Dialysis, Brain Stroke	Reactive Type 2 pneumocyte hyplerplasia	13662
LN8	COVID-19	N/A	N/A	N/A	Organising pneumonia	N/A
LN9	COVID-19	M	86	Prostate cancer, Abdominal Aortic Aneurysm, Giant Cells Arteritis	Organising pneumonia	11184
LN10	COVID-19	M	46	Dyslipidemia	Organising pneumonia	594
LN11	COVID-19	F	93	Type 2 Diabetes Mellitus, Systemic Arterial Hypertension, Dyslipidemia, Senile dementia	Acute phase DAD	6544

Supplemental Figure 1

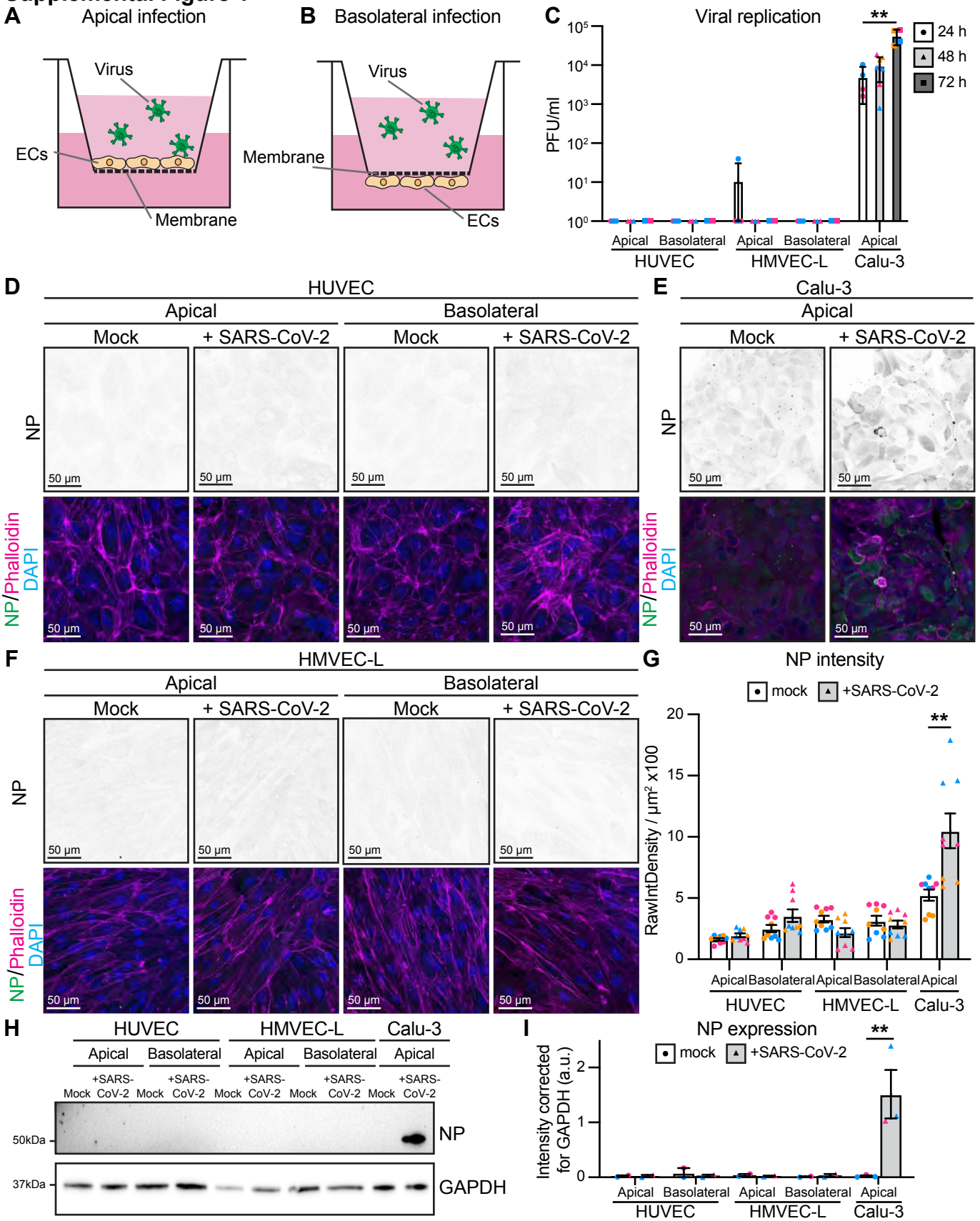

Supplemental Figure 2

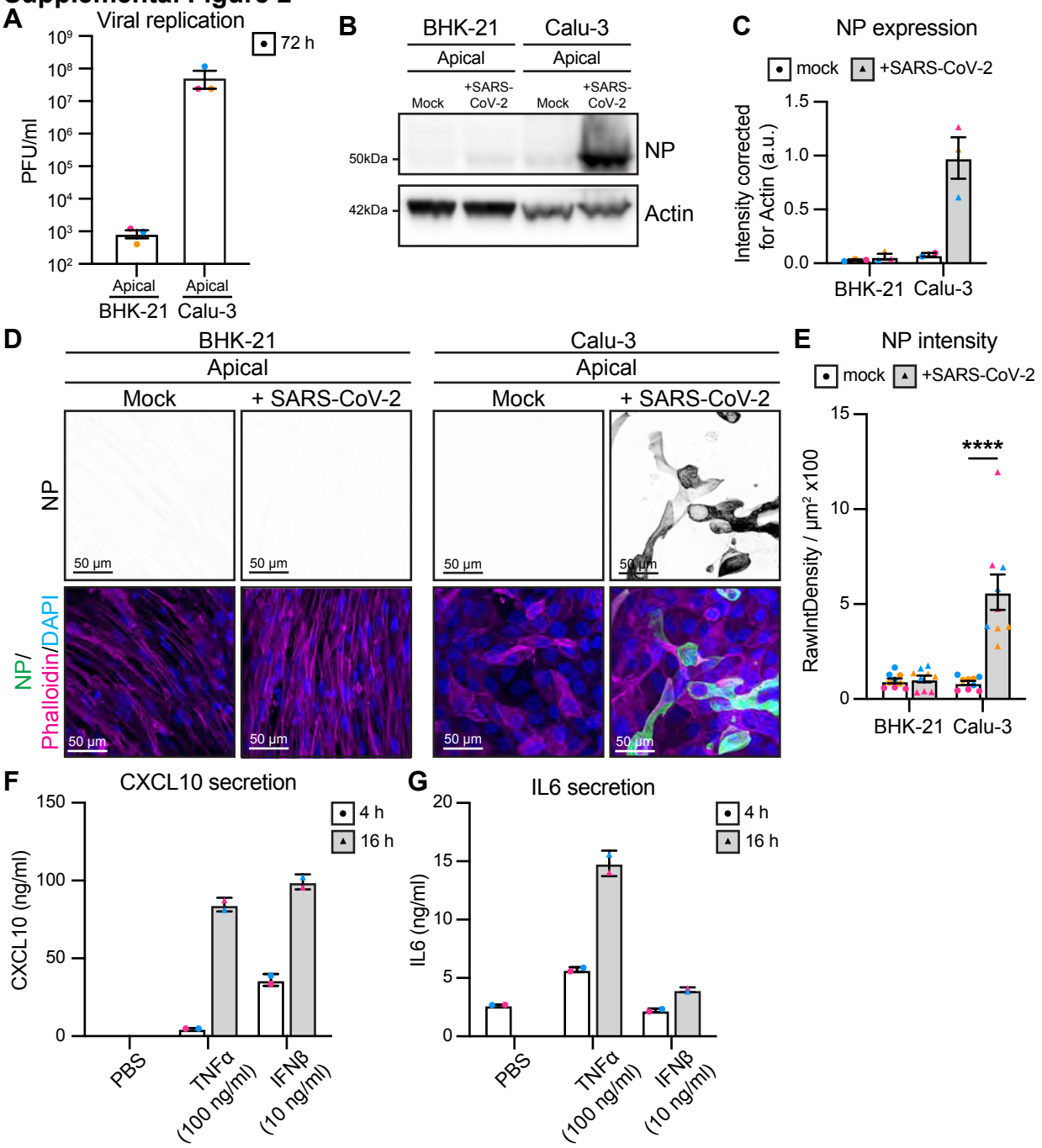

Supplemental Figure 3

Fig 2D top panel

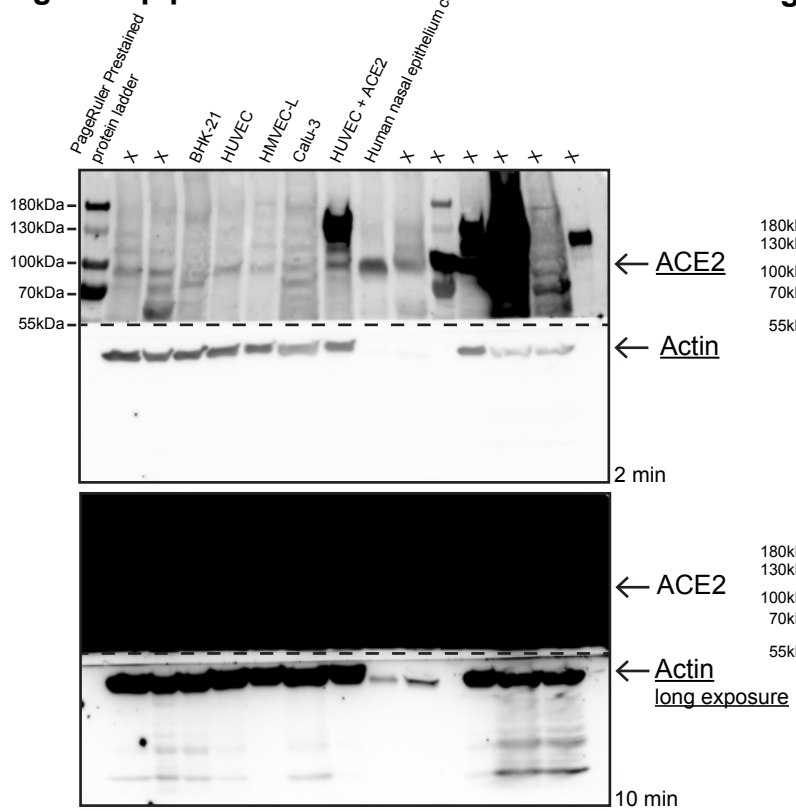

Fig 3D

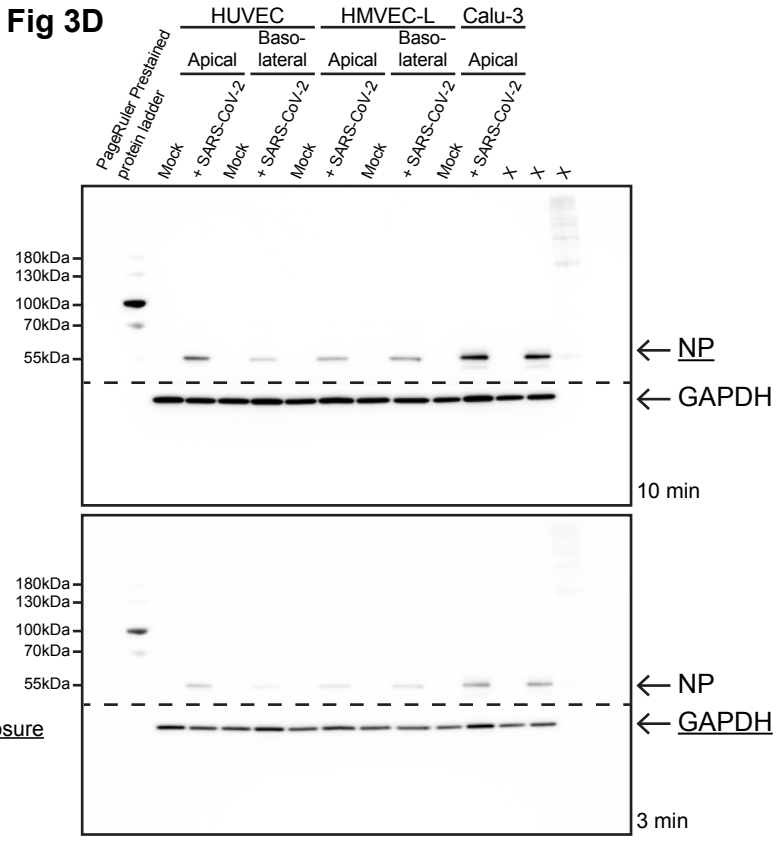

Fig 2D bottom panel

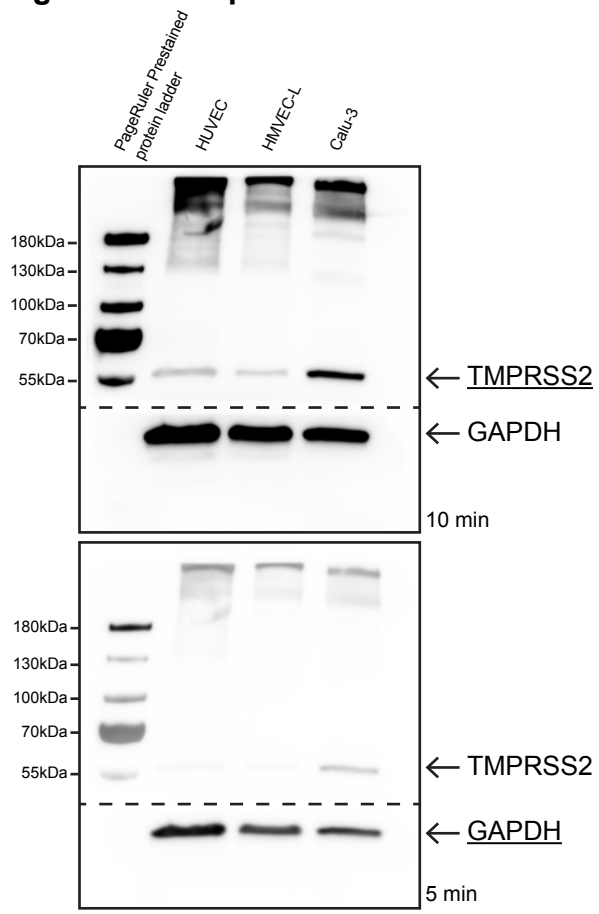

Fig 5D

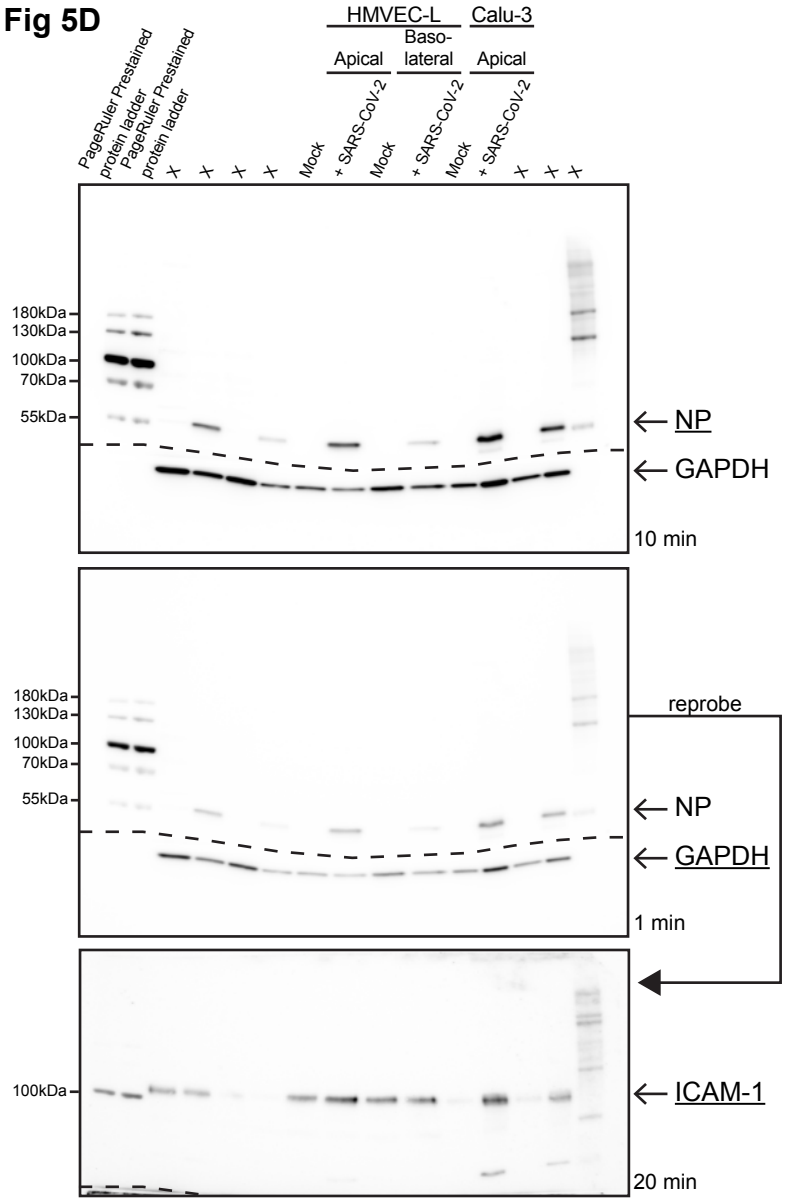

Supplemental Figure 3

Fig S1H

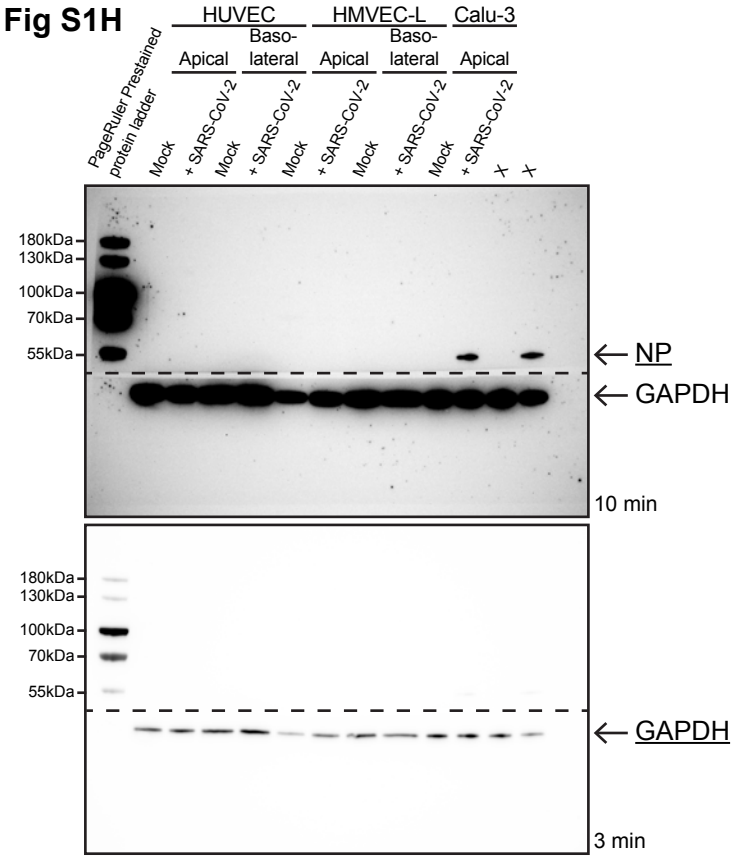
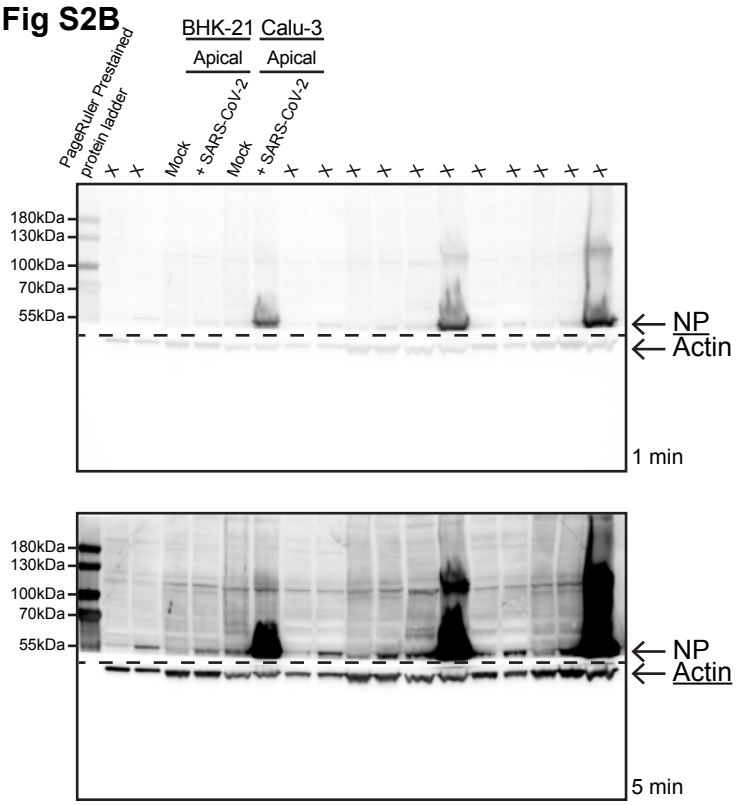
Fig S2B